Available online at www.sciencedirect.com
ScienceDirect
International Journal of Solids and Structures 45 (2008) 3466–3493
INTERNATIONAL JOURNAL OF SOLIDS AND STRUCTURES
www.elsevier.com/locate/ijsolstr

Linear viscoelastic analysis of straight and curved thin-walled laminated composite beams

Marcelo T. Piovan *, Víctor H. Cortínez

Centro de Investigaciones en Mecánica Teórica y Aplicada, Universidad Tecnológica Nacional FRBB, 11 de abril 461, B8000LMI, Bahía Blanca, BA, Argentina Consejo Nacional de Investigaciones Científicas y Technológicas (CONICET), Argentina

Received 6 June 2007; received in revised form 2 January 2008
Available online 20 February 2008

Abstract

This paper is devoted to study the behavior, in the range of linear viscoelasticity, of shear flexible thin-walled beam members constructed with composite laminated fiber-reinforced plastics. This work appeals to the correspondence principle in order to incorporate in unified model the motion equations of a curved or straight shear-flexible thin-walled beam member developed by the authors, together with the micromechanics and macromechanics of the reinforced plastic panels. Then, the analysis is performed in the Laplace or Carson domains. That is, the expressions describing the micromechanics and macromechanics of a plastic laminated composites and motion equations of the structural member are transformed into the Laplace or Carson domains where the relaxation components of the beam structure (straight or curved) are obtained. The resulting equations are numerically solved by means of finite element approaches defined in the Laplace or Carson domains. The finite element results are adjusted with a polynomial fitting. Then the creep behavior is obtained by means of a numerical technique for the inverse Laplace transform. Predictions of the present methodology are compared with experimental data and other approaches. New studies are performed focusing attention in the flexural–torsional behavior of shear flexible thin-walled straight composite beams as well as for thin-walled curved beams and frames.

Keywords: Thin-walled beams; Fiber-reinforced plastics; Shear flexibility; Linear viscoelasticity

1. Introduction

The use of slender composite structures is growing continuously in many applications of aeronautical, mechanical, naval and even construction industries. The composite materials have many advantages that motivate their use in structural applications. The most well-known features of composite materials are their high strength and stiffness properties along with low weight, good corrosion resistance, enhanced fatigue life, low thermal expansion properties among others (Barbero, 1999). Other important property of composite materials is the very low machining cost (Jones, 1999) in comparison with common isotropic materials, i.e.

* Corresponding author. Tel.: +54 291 4555220; fax: +54 291 4555311.
E-mail address: mpiovan@frbb.utn.edu.ar (M.T. Piovan).

0020-7683/$ - see front matter © 2008 Elsevier Ltd. All rights reserved.
doi:10.1016/j.ijsolstr.2008.02.009

steel and aluminum. As a consequence of the increasing applications of thin-walled beams constructed with curved or straight shapes, many research activities have been devoted toward the development of theoretical and computational methods for the appropriate analysis of such members.

In the past years, many structural models have been introduced to evaluate the mechanics of composite thin-walled beams members under general static loads in the linear elastic range. Interesting models for linear static analysis of thin-walled composite straight beams can be found in the works of Pollock and Sack (1995), Barbero et al. (1993), Massa and Barbero (1998) and Kim and White (1997) among others. These models were developed on the basis of shear-flexibility concepts. The work of Yu et al. (2005) and Volovoi et al. (1999a) offers a good background for the case of Vlasov approaches of composite thin-walled straight beams. Although most of mentioned models were derived taking into account warping (Pollock and Sack, 1995; Barbero et al., 1993; Massa and Barbero, 1998), flexural–torsional coupling and including shear flexibility due to bending, none of them was developed considering also the shear flexibility due to torsion-warping, that can be important in some circumstances (which involve different stacking sequences, slenderness characteristics, type of cross-section, etc). In recent years, the authors have developed models (Cortínez and Piovan, 2002; Piovan and Cortínez, 2003, 2007a; Piovan, 2003) for curved and straight thin-walled beams accounting for comprehensive shear flexibility. That is, the shear flexibility is composed by the conventional terms due to bending or flexure and the non-conventional term of warping torsion. It has been proved; that the inclusion of the shear flexibility due to warping-torsion is crucial for the appropriate prediction of displacements and deformations in elastically coupled thin-walled beams (Piovan and Cortínez, 2007a; Piovan, 2003). The aforementioned approaches (Pollock and Sack, 1995; Barbero et al., 1993; Massa and Barbero, 1998; Piovan and Cortínez, 2003a, 2007a) are quite useful in linear static's, however by themselves cannot allow the possibility to study the behavior, for a given load, of progressive deformations along the time or the long-term structural response. Under this behavior, also known as "creep effect", the displacements and deformations of the structure reach such a value that can eventually lead to the structural catastrophic collapse. This aspect is important in plastic reinforced structures subjected to changes in environmental features such as humidity or temperature. Examples of these circumstances are bridges, pultruded profiles for out-door applications, etc. The viscoelasticity concept offers the possibility to describe and analyse the creep behavior of composite structural material.

The structures constructed with laminated fiber-reinforced plastics are quite susceptible to suffer progressive deformations along the time, principally due to the viscoelastic features in the matrix of the composite material. Under these circumstances, it is of crucial importance the proper understanding of the viscoelastic properties of composite plastic materials and their characterization in order to analyse the behavior of structural components. Thus, Barbero and Luciano (1995) developed a micromechanical model, to characterize linear viscoelastic solids with periodic microstructure. They deduced the analytical expressions, in the Laplace domain, for the linear relaxation tensor of the matrix of a composite material whose viscoelastic behavior is considered with a Maxwel–Voigt model (Mase, 1977) with four-parameters. The previous micromechanical model (Barbero and Luciano, 1995) was employed by Harris and Barbero (1998) together with a macromechanical model to predict the viscoelastic behavior of laminated composites under tensile loads. Qiao et al. (2000) performed a study about linear viscoelastic thin-walled composite beams, describing the micromechanical model (Barbero and Luciano, 1995) in the Carson domain and assuming that the matrix of the composite material has linear viscoelastic behavior described according to a Maxwell model (Mase, 1977) with two-parameters. In Barbero and Luciano (1995), as well as in Harris and Barbero (1998) and in Qiao et al. (2000) new studies and comparisons with experiments have been made, showing a good correlation between the predictions of the models and the experiments.

Although there is evidence of studies about linear viscoelastic analysis of thin-walled beams (Harris and Barbero, 1998; Qiao et al., 2000; Lee and Ueng, 1995), most of them consider only axial or bending motions based on structural models for straight beams taking into account only shear flexibility due to bending. Recently, Oliveira and Creus (2003) developed a study of viscoelastic thin-walled straight beams by means of a non-linear approach using finite shell elements. On the other hand, in the knowledge of the authors there is no evidence of research on the linear viscoelastic behavior of thin-walled composite curved beams.

In the present article, a study on the linear viscoelastic behavior of thin-walled curved and straight beams constructed with composite materials of polymeric matrix. The micromechanical model derived by Barbero and Luciano (1995) is applied to a thin-walled curved beam model allowing for full shear flexibility derived

by the authors (Piovan and Cortínez, 2003a, 2007b). It has to be mentioned that the curved beam model (Piovan and Cortínez, 2003a, 2007b) can be reduced to the straight case if one employs the condition of infinity curvature radius. After a brief review of the micromechanical model (Barbero and Luciano, 1995) that describes the linear viscoelastic behavior of the polymeric matrix, the macromechanical model for the curved-straight beam is introduced and described in the Carson domain. Then, the scheme of solution based on the method of finite elements is introduced. A finite element with four-nodes is employed in the computational task. The linear viscoelastic response of the structure is calculated in the Carson domain by means of the aforementioned finite element. The creep behavior in the time domain is obtained by means of a numerical procedure in the inverse Laplace transformation together with a procedure of polynomial adjustment of the previous finite element results. Comparisons of the present model reduced to previous simplified approaches and with experimental results are performed. New studies are performed attending particularly the flexural–torsional behavior of shear flexible thin-walled straight composite beams and especially for thin-walled curved beams. Thus, the methodology is employed to explore the influence of creep effect in different stacking sequences, cross-sectional shapes and in-plane or out-of-plane motions of thin-walled curved beams.

2. Description of the macromechanical model

2.1. Brief review of the basics of the linear viscoelastic behavior for polymeric composites

The viscoelastic behavior of a polymeric composite material with periodic microstructure has been evaluated analytically and experimentally by Barbero and Luciano (1995) and Luciano and Barbero (1994, 1995). In these works, it was observed that the viscoelastic behavior of composite materials is exclusively due to the polymeric matrix instead of the reinforcement fibers, because the creep effect does not have a measurable influence in the fibers, thus allowing the consideration of the fibers behavior as elastic. Also, the time variation of Poisson's ratios of matrix and fibers is quite difficult to be measured and consequently with the literature (Aboudi, 1991) those coefficients are assumed invariable with the time. This criterion simplifies the expressions in the derivation process without affecting the most relevant conceptual issues for the modeling procedure of the linear viscoelastic relaxation components. On the other hand, this simplification showed to correlate quite well with the available experimental data. For the interested reader on this particular subject, in the open literature (Aboudi, 1991; Luciano and Barbero, 1994, 1995; Barbero, 2007) clarifying topics and examples can be found. Under these circumstances the micromechanical model for linear viscoelastic polymeric composites is subjected to the following hypotheses (Barbero and Luciano, 1995):

H1: The polymeric matrix of the composite material has a linear viscoelastic behavior whereas the fibers are supposed to behave elastically.
H2: The viscoelastic behavior of the matrix can be represented by means of simple spring-dashpot Maxwell family models (Mase, 1977) to account only for secondary creep (with a two-parameter model) or to consider both primary and secondary creep (with a four-parameters model).
H3: The Poisson's ratios for fibers and polymeric matrix are considered constants.
H4: The composite material is assumed to be transversely isotropic.

The constitutive equations for a linear viscoelastic material can be obtained from experimental tests in the absence of initial stresses or strains before the loading process. Then, strains and stresses as functions of the time can be represented in the following form:

$$\varepsilon(t) = \mathcal{M}(t)\sigma \tag{1}$$

$$\sigma(t) = \mathcal{L}(t)\varepsilon \tag{2}$$

where $\mathcal{M}(t)$ and $\mathcal{L}(t)$ are the functions of "creep compliance" and "relaxation", which are obtained from tests of creep and relaxation, respectively. In fact, a creep test allows obtaining the creep compliance function $\mathcal{M}(t)$ for a given level of constant stress. If the function $\mathcal{M}(t)$ is independent of the stress level, then it represents a

linear viscoelastic material. On the other hand, with the relaxation test one can obtain the relaxation function $\mathcal{L}(t)$ for a given level of constant strain.

Now appealing to the Correspondence Principle – which can be employed to make an analogy between the elastic and linear viscoelastic relaxation moduli of heterogeneous materials that have the same phase geometry (Mase, 1977) – one can find a relationship between functions $\mathcal{L}(t)$ and $\mathcal{M}(t)$. The transformation of a generic function of time $G(t)$ in the Carson domain (Laws and McLaughlin, 1978) is described as follows:

$$\widehat{\mathcal{G}}(\widehat{s}) = O_C[G(t)] = \widehat{s}\int_0^\infty \mathrm{e}^{-\widehat{s}\,t} G(t)\,\mathrm{d}t = \widehat{s}\;\widehat{G}(\widehat{s}) = \widehat{s}\;O_{\mathcal{L}}[G(t)] \tag{3}$$

where $\widehat{s}$ is the variable of the Carson or Laplace domains, $\widehat{G}(\widehat{s})$ is the Laplace Transform of function $G(t)$ and $O_{\mathcal{L}}[G(t)]$ and $O_C[G(t)]$ are the Laplace and Carson transformation operators, respectively.

Then, taking into account (3) in expressions (1) and (2), it is possible to arrive (Qiao et al., 2000; Luciano and Barbero, 1994, 1995) to the following relationship between the transformed creep compliance and relaxation functions:

$$\widehat{\mathcal{L}}(\widehat{s})\,\widehat{\mathcal{M}}(\widehat{s}) = 1 \tag{4}$$

Expression (4) can be employed to obtain the effective relaxation modulus $\mathcal{L}(t)$ if the creep compliance $\mathcal{M}(t)$ is known.

Now the creep compliances for a two-parameter Maxwell (Qiao et al., 2000) model and for a four-parameter Maxwell–Voigt model, also called Maxwell–Kelvin model (Mase, 1977; Luciano and Barbero, 1995) are described in the following functions of time:

$$\mathcal{M}(t) = \frac{1}{E^{(M)}} + \frac{t}{\eta^{(M)}} \tag{5}$$

$$\mathcal{M}(t) = \frac{1}{E^{(e)}} + \frac{t}{\eta^{(M)}} + \frac{1}{E^{(V)}}\left(1 - \mathrm{Exp}\left[-\frac{E^{(V)}t}{\eta^{(V)}}\right]\right) \tag{6}$$

In (5) and (6) $1/\eta^{(M)}$ is the slope of the secondary creep, as one can see in Fig. 1. In (5) $1/\mathrm{E}^{(M)}$ represents the strain deformation lumped at time $t = 0$. In (6) $E^{(e)}$ and $E^{(V)}$ are elastic moduli and together with $\eta^{(V)}$ describe the primary creep. Transforming (5) and (6) to the Carson domain and taking into account (4) it is possible to arrive to the expressions of the effective relaxation modulus of the linear viscoelastic matrix employing the Maxwell model and the Maxwell–Voigt model, respectively:

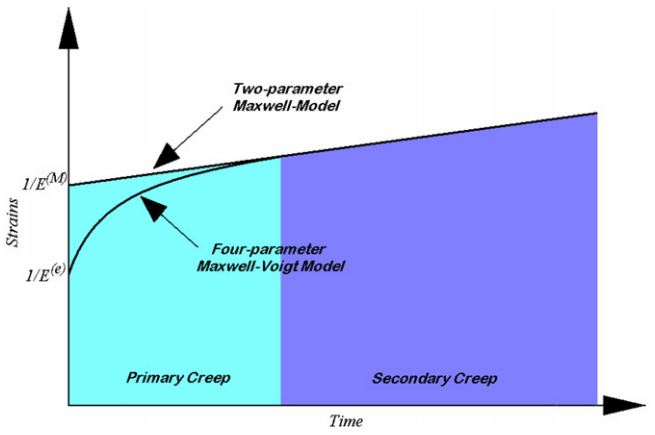

Fig. 1. Representation of the creep pattern.

$$\widehat{E}_M = \widehat{\mathcal{L}}(\widehat{s}) = \frac{1}{\widehat{\mathcal{M}}(\widehat{s})} = \frac{E^{(M)}\eta^{(M)}\,\widehat{s}}{(E^{(M)} + \eta^{(M)}\,\widehat{s})} \tag{7}$$

$$\widehat{E}_M = \widehat{\mathcal{L}}(\widehat{s}) = \frac{1}{\widehat{\mathcal{M}}(\widehat{s})} = \frac{E^{(e)}\eta^{(M)}\left(E^{(V)} + \eta^{(V)}\,\widehat{s}\right)\widehat{s}}{E^{(e)}E^{(V)} + \left(E^{(V)}\eta^{(M)} + E^{(e)}(\eta^{(V)} + \eta^{(M)})\right)\widehat{s} + \eta^{(V)}\eta^{(M)}\,\widehat{s}^2} \tag{8}$$

The expression (7) shows a good correlation with experimental data when only the secondary creep is of interest (Qiao et al., 2000; Harris and Barbero, 1998). On the other hand expression (8) reflects a very good agreement with experimental results for the primary and secondary creep in view of the work of Luciano and Barbero (1994). Expressions (7) or (8) imply that the overall structural beam model can be suited for a two-parameter or four-parameter viscoelastic model depending on the experimental data available that characterizes a particular specimen of composite material.

The expressions of the Lamé properties for the matrix can be described in terms of the effective relaxation modulus E_M as shown in (9). The expressions of the Lamé properties for the elastic fibers are represented in (10).

$$\widehat{\lambda}_M = \frac{\widehat{E}_M \nu_M}{(1+\nu_M)(1-2\nu_M)}, \quad \widehat{\mu}_M = \frac{\widehat{E}_M}{2(1+\nu_M)} \tag{9.a, b}$$

$$\lambda_F = \frac{E_F \nu_F}{(1+\nu_F)(1-2\nu_F)}, \quad \mu_F = \frac{E_F}{2(1+\nu_F)} \tag{10.a, b}$$

In expressions (9) and (10), ν_F, ν_M and E_F are Poisson coefficient of fiber, Poisson coefficient of matrix and Elastic modulus of the fibers, respectively. Remember that these properties are constants according to the hypotheses H1 and H3. Note also that Lamé properties of the fibers are constants.

The components of the relaxation tensor for transversely isotropic material can be represented with the following expressions (Qiao et al., 2000):

$$\begin{aligned}
&\widehat{C}_{11} = \widehat{\mathcal{L}}_{11}, \quad \widehat{C}_{12} = \widehat{\mathcal{L}}_{12}, \quad \widehat{C}_{66} = \widehat{\mathcal{L}}_{66} \\
&\widehat{C}_{22} = \frac{3}{4}\widehat{\mathcal{L}}_{22} + \frac{1}{4}\widehat{\mathcal{L}}_{23} + \frac{1}{2}\widehat{\mathcal{L}}_{44} \\
&\widehat{C}_{23} = \frac{1}{4}\widehat{\mathcal{L}}_{22} + \frac{3}{4}\widehat{\mathcal{L}}_{23} - \frac{1}{2}\widehat{\mathcal{L}}_{44} \\
&\widehat{C}_{44} = \frac{1}{4}\widehat{\mathcal{L}}_{22} - \frac{1}{4}\widehat{\mathcal{L}}_{23} + \frac{1}{2}\widehat{\mathcal{L}}_{44}
\end{aligned} \tag{11}$$

where $\widehat{\mathcal{L}}_{ij}$ are the components of the relaxation tensor of a linear viscoelastic polymeric solid with long reinforcing fibers oriented in the principal direction. These components depend on the Lamé properties of fibers and matrix and the fiber volume fraction V_F. The expressions of the relaxation components $\mathcal{L}_{ij}$ were introduced by Luciano and Barbero (1994).

The unidirectional plies are modeled with the assumption of a plane stress state, that is:

$$\begin{Bmatrix} \widehat{\sigma}_{11} \\ \widehat{\sigma}_{22} \\ \widehat{\sigma}_{12} \end{Bmatrix} = \begin{bmatrix} \widehat{Q}^*_{11} & \widehat{Q}^*_{12} & 0 \\ \widehat{Q}^*_{12} & \widehat{Q}^*_{22} & 0 \\ 0 & 0 & \widehat{Q}^*_{66} \end{bmatrix} \begin{Bmatrix} \widehat{\varepsilon}_{11} \\ \widehat{\varepsilon}_{22} \\ \widehat{\gamma}_{12} \end{Bmatrix} \tag{12}$$

where the reduced relaxation components $\widehat{Q}^*_{ij}$ are given by:

$$\widehat{Q}^*_{11} = \widehat{C}_{11} - \frac{\widehat{C}^2_{12}}{\widehat{C}_{22}}, \quad \widehat{Q}^*_{12} = \widehat{C}_{12} - \frac{\widehat{C}_{12}\widehat{C}_{23}}{\widehat{C}_{22}}, \quad \widehat{Q}^*_{22} = \widehat{C}_{22} - \frac{\widehat{C}^2_{23}}{\widehat{C}_{22}}, \quad \widehat{Q}^*_{66} = \widehat{C}_{66} \tag{13}$$

If the stacking sequence of a segment of the cross-section has a layer with continuous strand mat (CSM) which is transversely isotropic, then expression (12) can be written as:

$$\begin{Bmatrix} \widehat{\sigma}_{11} \\ \widehat{\sigma}_{22} \\ \widehat{\sigma}_{12} \end{Bmatrix} = \begin{bmatrix} \widehat{\bar{Q}}^{*}_{11}\big|_{\mathrm{CSM}} & \widehat{\bar{Q}}^{*}_{12}\big|_{\mathrm{CSM}} & 0 \\ \widehat{\bar{Q}}^{*}_{12}\big|_{\mathrm{CSM}} & \widehat{\bar{Q}}^{*}_{22}\big|_{\mathrm{CSM}} & 0 \\ 0 & 0 & \widehat{\bar{Q}}^{*}_{66}\big|_{\mathrm{CSM}} \end{bmatrix} \begin{Bmatrix} \widehat{\varepsilon}_{11} \\ \widehat{\varepsilon}_{22} \\ \widehat{\gamma}_{12} \end{Bmatrix} \tag{14}$$

where the $\widehat{\bar{Q}}^{*}_{ij}\big|_{\mathrm{CSM}}$ are given by the following expressions obtained by Harris and Barbero (1998):

$$\begin{aligned} \widehat{\bar{Q}}^{*}_{11}\big|_{\mathrm{CSM}} &= \frac{3}{8}\widehat{\bar{Q}}^{*}_{11} + \frac{2}{8}\widehat{\bar{Q}}^{*}_{12} + \frac{3}{8}\widehat{\bar{Q}}^{*}_{22} + \frac{4}{8}\widehat{\bar{Q}}^{*}_{66} \\ \widehat{\bar{Q}}^{*}_{12}\big|_{\mathrm{CSM}} &= \frac{1}{8}\widehat{\bar{Q}}^{*}_{11} + \frac{6}{8}\widehat{\bar{Q}}^{*}_{12} + \frac{1}{8}\widehat{\bar{Q}}^{*}_{22} - \frac{4}{8}\widehat{\bar{Q}}^{*}_{66} \\ \widehat{\bar{Q}}^{*}_{22}\big|_{\mathrm{CSM}} &= \frac{3}{8}\widehat{\bar{Q}}^{*}_{11} + \frac{2}{8}\widehat{\bar{Q}}^{*}_{12} + \frac{3}{8}\widehat{\bar{Q}}^{*}_{22} + \frac{4}{8}\widehat{\bar{Q}}^{*}_{66} \\ \widehat{\bar{Q}}^{*}_{66}\big|_{\mathrm{CSM}} &= \frac{1}{8}\widehat{\bar{Q}}^{*}_{11} - \frac{2}{8}\widehat{\bar{Q}}^{*}_{12} + \frac{1}{8}\widehat{\bar{Q}}^{*}_{22} + \frac{4}{8}\widehat{\bar{Q}}^{*}_{66} \end{aligned} \tag{15}$$

The expressions (12) and (14) can be employed in the usual form (Jones, 1999; Barbero, 1999) to calculate the relaxation components for the laminates of the cross-sectional panels.

2.2. Description of the structural model in the Carson domain

In this paragraph, a structural model of composite thin-walled curved beams developed earlier by the authors (Piovan and Cortínez, 2003a; Piovan, 2003) is reformulated in the Carson domain in order to perform studies about the linear viscoelastic response of curved thin-walled beams with polymeric matrix. Fig. 2(a) shows an overall description of the curved beam. In Fig. 2(b) one can see two reference systems. The principal reference system is located at point ***C***, whereas an auxiliary reference system is located at point ***A***. The motion variables are measured with respect to the point ***C***. The basic constitutive equations for the laminates are referenced from point ***A***.

Thus, the strains of a laminated plate of the curved thin-walled composite beam can be represented in the Carson domain as:

$$\widehat{\varepsilon}_{xx} = [\widehat{\varepsilon}_{D1} - Y(s)\widehat{\varepsilon}_{D3} - Z(s)\widehat{\varepsilon}_{D2} - \widehat{\omega}_p(s,\widehat{s})\widehat{\varepsilon}_{D4}]\mathcal{F} \tag{16.a}$$

$$\widehat{\kappa}_{xx} = \left[\frac{\mathrm{d}Z}{\mathrm{d}s}\widehat{\varepsilon}_{D3} - \frac{\mathrm{d}Y}{\mathrm{d}s}\widehat{\varepsilon}_{D2} - l(s)\widehat{\varepsilon}_{D4}\right]\mathcal{F} \tag{16.b}$$

$$\widehat{\gamma}_{xs} = \left[\frac{\mathrm{d}Y}{\mathrm{d}s}\widehat{\varepsilon}_{D5} + \frac{\mathrm{d}Z}{\mathrm{d}s}\widehat{\varepsilon}_{D6} + [r(s) + \widehat{\psi}(s,\widehat{s})]\widehat{\varepsilon}_{D7} + \widehat{\psi}(s,\widehat{s})\widehat{\varepsilon}_{D4}\right]\mathcal{F} \tag{16.c}$$

$$\widehat{\kappa}_{xs} = [-2\widehat{\varepsilon}_{D8} + \widehat{\varepsilon}_{D7}]\mathcal{F} \tag{16.d}$$

The generalized deformations $\widehat{\varepsilon}_{D1}$, $\widehat{\varepsilon}_{D2}$, $\widehat{\varepsilon}_{D3}$, $\widehat{\varepsilon}_{D4}$, $\widehat{\varepsilon}_{D5}$, $\widehat{\varepsilon}_{D6}$, $\widehat{\varepsilon}_{D7}$ and $\widehat{\varepsilon}_{D8}$ are given in terms of the beam displacements represented in the Carson domain in the following form:

$$\widehat{\varepsilon}_{D1} = \left(\frac{\partial\widehat{u}_{xc}}{\partial x} + \frac{\widehat{u}_{yc}}{R}\right), \quad \widehat{\varepsilon}_{D2} = \left(\frac{\partial\widehat{\theta}_y}{\partial x} + \frac{\widehat{\phi}_x}{R}\right), \quad \widehat{\varepsilon}_{D3} = \left(\frac{\partial\widehat{\theta}_z}{\partial x} - \frac{1}{R}\frac{\partial\widehat{u}_{xc}}{\partial x}\right), \quad \widehat{\varepsilon}_{D4} = \left(\frac{\partial\widehat{\theta}_x}{\partial x} - \frac{1}{R}\frac{\partial\widehat{\theta}_y}{\partial x}\right) \tag{17.a – d}$$

$$\widehat{\varepsilon}_{D5} = \left(\frac{\partial\widehat{u}_{yc}}{\partial x} - \widehat{\theta}_z\right), \quad \widehat{\varepsilon}_{D6} = \left(\frac{\partial\widehat{u}_{zc}}{\partial x} - \widehat{\theta}_y\right), \quad \widehat{\varepsilon}_{D7} = \left(\frac{\partial\widehat{\phi}_x}{\partial x} - \widehat{\theta}_x\right), \quad \widehat{\varepsilon}_{D8} = \left(\frac{\partial\widehat{\phi}_x}{\partial x} - \frac{\widehat{\theta}_y}{R}\right) \tag{18.a – d}$$

where u_{xc} is the axial displacement of the cross-section, θ_z and θ_y are bending rotation parameters (if the curved beam is reduced to the case of a straight beam, these parameters are the bending rotations), u_{yc} and u_{zc} are the transversal bending displacements of the cross-section, ϕ_x is the twisting angle and θ_x is a measure of the warping intensity. In expressions (16) the entities $Y(s)$, Z(s), $r(s)$ and $l(s)$ are geometric cross-sectional parameters – see Fig. 2(b) – that have no changes in the time.

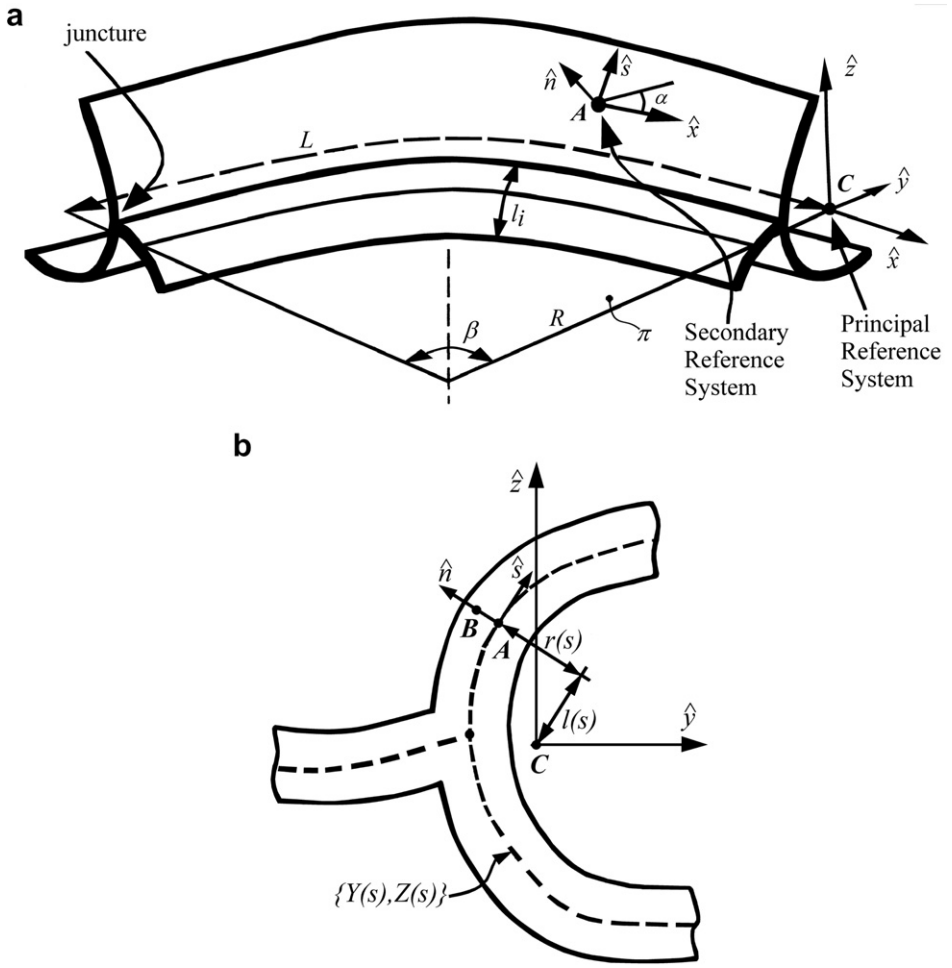

Fig. 2. Structural member. (a) General layout. (b) Cross-section.

The functions $\mathcal{F}$, $r(s)$ and $l(s)$ are defined (Piovan and Cortínez, 2003a) as follows:

$$\mathcal{F} = \frac{R}{R + Y(s)}, \quad r(s) = Z(s)\frac{\mathrm{d}Y}{\mathrm{d}s} - Y(s)\frac{\mathrm{d}Z}{\mathrm{d}s}, \quad l(s) = Y(s)\frac{\mathrm{d}Y}{\mathrm{d}s} + Z(s)\frac{\mathrm{d}Z}{\mathrm{d}s} \tag{19.a–c}$$

Whereas the functions $\widehat{\omega}_p(s, \widehat{s})$ and $\widehat{\psi}(s, \widehat{s})$ are defined in the following form:

$$\widehat{\omega}_p(s, \widehat{s}) = \int_s [r(s) + \widehat{\psi}(s, \widehat{s})]\,\mathrm{d}s - \frac{\oint_S [r(s) + \widehat{\psi}(s, \widehat{s})]\widehat{\overline{A}}_{11}(s)\,\mathrm{d}s}{\oint_S \widehat{\overline{A}}_{11}(s)\,\mathrm{d}s} \tag{20}$$

$$\widehat{\psi}(s, \widehat{s}) = \frac{1}{\widehat{\overline{A}}_{66}(s)}\left[\frac{\int_s r(s)\,\mathrm{d}s}{\oint_S \frac{1}{\widehat{\overline{A}}_{66}(s)}\,\mathrm{d}s}\right] \tag{21}$$

It is important to note that s and $\widehat{s}$ are inherently different because the first one is the geometric co-ordinate in the circumferential direction, whereas the second one is the variable of the Carson domain. Expression (20) holds for both open and closed cross-sections, because in the case of open cross-sections, it is verified the condition $\psi(s, \widehat{s}) = 0$ (Piovan, 2003). The coefficients $\overline{A}_{11}$ and $\overline{A}_{66}$ are modified relaxation coefficients in the Carson domain (Piovan and Cortínez, 2007a).

The constitutive equations, in the Carson domain, of the beam stress-resultants in terms of the generalized deformations are given by:

$$\begin{Bmatrix} \widehat{Q}_X \\ \widehat{\mathcal{M}}_Y \\ \widehat{\mathcal{M}}_Z \\ \widehat{B} \\ \widehat{Q}_Y \\ \widehat{Q}_Z \\ \widehat{T}_W \\ \widehat{T}_{SV} \end{Bmatrix} = \begin{bmatrix} \widehat{\overline{J}}^{11}_{11} & \widehat{\overline{J}}^{11}_{12} & \widehat{\overline{J}}^{11}_{13} & \widehat{\overline{J}}^{11}_{14} & \widehat{\overline{J}}^{16}_{15} & \widehat{\overline{J}}^{16}_{16} & \widehat{\overline{J}}^{16}_{17} & \widehat{\overline{J}}^{16}_{18} \\ & \widehat{\overline{J}}^{11}_{22} & \widehat{\overline{J}}^{11}_{23} & \widehat{\overline{J}}^{11}_{24} & \widehat{\overline{J}}^{16}_{25} & \widehat{\overline{J}}^{16}_{26} & \widehat{\overline{J}}^{16}_{27} & \widehat{\overline{J}}^{16}_{28} \\ & & \widehat{\overline{J}}^{11}_{33} & \widehat{\overline{J}}^{11}_{34} & \widehat{\overline{J}}^{16}_{35} & \widehat{\overline{J}}^{16}_{36} & \widehat{\overline{J}}^{16}_{37} & \widehat{\overline{J}}^{16}_{38} \\ & & & \widehat{\overline{J}}^{11}_{44} & \widehat{\overline{J}}^{16}_{45} & \widehat{\overline{J}}^{16}_{46} & \widehat{\overline{J}}^{16}_{47} & \widehat{\overline{J}}^{16}_{48} \\ & & & & \widehat{\overline{J}}^{66}_{55} & \widehat{\overline{J}}^{66}_{56} & \widehat{\overline{J}}^{66}_{57} & \widehat{\overline{J}}^{66}_{58} \\ & & \text{sym} & & & \widehat{\overline{J}}^{66}_{66} & \widehat{\overline{J}}^{66}_{67} & \widehat{\overline{J}}^{66}_{68} \\ & & & & & & \widehat{\overline{J}}^{66}_{77} & \widehat{\overline{J}}^{66}_{78} \\ & & & & & & & \widehat{\overline{J}}^{66}_{88} \end{bmatrix} \begin{Bmatrix} \widehat{\varepsilon}_{D1} \\ -\widehat{\varepsilon}_{D2} \\ -\widehat{\varepsilon}_{D3} \\ -\widehat{\varepsilon}_{D4} \\ \widehat{\varepsilon}_{D5} \\ \widehat{\varepsilon}_{D6} \\ \widehat{\varepsilon}_{D7} \\ \widehat{\varepsilon}_{D8} \end{Bmatrix} \tag{22}$$

where $\widehat{Q}_X$, $\widehat{M}_Y$, $\widehat{M}_Z$, $\widehat{B}$, $\widehat{Q}_Y$, $\widehat{Q}_Z$, $\widehat{T}_W$ and $\widehat{T}_{SV}$ are the beam stress-resultants transformed into the Carson domain. Q_X is the axial force; M_Y and M_Z are the bending moments; B is the bi-moment; Q_Y and Q_Z are the shear forces; T_W is the flexural–torsional moment and T_{SV} is the twisting moment of Saint-Venant torsion.

The matrix in expression (22) has to be considered as the matrix of relaxation coefficients $\widehat{\overline{J}}^{hk}_{ij}$ of the beam. These coefficients are given by the following form:

$$\widehat{\overline{J}}^{kh}_{ij} = \int_S \widehat{\overline{A}}_{kh}(\widehat{\overline{g}}^{(b)}_i \widehat{\overline{g}}^{(b)}_j)\,\mathrm{d}s + \int_S \widehat{\overline{B}}_{kh}(\widehat{\overline{g}}^{(b)}_i \widehat{\overline{g}}^{(d)}_j + \widehat{\overline{g}}^{(d)}_i \widehat{\overline{g}}^{(b)}_j)\,\mathrm{d}s + \int_S \widehat{\overline{D}}_{kh}(\widehat{\overline{g}}^{(d)}_i \widehat{\overline{g}}^{(d)}_j)\,\mathrm{d}s \tag{23}$$

for $i = 1,\ldots,8$; $j = 1,\ldots,8$; $\{h,k\} = \{1,6\}$ and with:

$$\widehat{\overline{g}}^{(b)} = \left\{1, Z(s), Y(s), \widehat{\omega}_p(s,\widehat{s}), \frac{\mathrm{d}Y}{\mathrm{d}s}, \frac{\mathrm{d}Z}{\mathrm{d}s}, r(s) + \widehat{\psi}(s,\widehat{s}), \widehat{\psi}(s,\widehat{s})\right\} \tag{24.a}$$

$$\widehat{\overline{g}}^{(c)} = \left\{0, 0, 0, 0, \frac{\mathrm{d}Z}{\mathrm{d}s}, -\frac{\mathrm{d}Y}{\mathrm{d}s}, -l(s), 0\right\} \tag{24.b}$$

$$\widehat{\overline{g}}^{(d)} = \left\{0, \frac{\mathrm{d}Y}{\mathrm{d}s}, -\frac{\mathrm{d}Z}{\mathrm{d}s}, l(s), 0, 0, 1, -2\right\} \tag{24.c}$$

The coefficients $\widehat{\overline{A}}_{kh}$, $\widehat{\overline{B}}_{kh}$ and $\widehat{\overline{D}}_{kh}$ are modified relaxation coefficients in the Carson domain. These coefficients are obtained employing (12) or (14) in the general constitutive relation between resultant forces and moments and mid-surface strains and curvatures, and neglecting (Piovan and Cortínez, 2003a) the circumferential resultant force and moment (i.e. $N_{SS} = M_{SS} = 0$) and rearranging the remaining equations. This simplification in the constitutive equations proved to offer good correlation of the curved/straight beam model predictions with the experimental results in the linear elastic range (Piovan, 2003; Piovan and Cortínez, 2007a). If the stacking sequence is especially orthotropic or symmetric balanced or quasi-isotropic the constitutive matrix in (22) can be simplified because the only non-vanishing components are those of the diagonal and $\overline{J}^{66}_{78}$ (Piovan, 2003).

Finally the equations of static equilibrium of the curved thin-walled composite beam are rewritten in the Carson domain as it follows:

$$-\frac{\partial}{\partial x}\left[\widehat{Q}_X+\frac{\widehat{\mathcal{M}}_Z}{R}\right]-\widehat{q}_1(x,\widehat{s})=0 \tag{25.a}$$

$$-\frac{\partial\widehat{Q}_Y}{\partial x}+\frac{\widehat{Q}_X}{R}-\widehat{q}_2(x,\widehat{s})=0 \tag{25.b}$$

$$\frac{\partial\widehat{\mathcal{M}}_Z}{\partial x}-\widehat{Q}_Y-\widehat{q}_3(x,\widehat{s})=0 \tag{25.c}$$

$$-\frac{\partial\widehat{Q}_Z}{\partial x}-\widehat{q}_4(x,\widehat{s})=0 \tag{25.d}$$

$$\frac{\partial}{\partial x}\left[\widehat{\mathcal{M}}_Y-\frac{\widehat{B}}{\widehat{R}}\right]-\widehat{Q}_Z-\frac{\widehat{T}_{SV}}{R}-\widehat{q}_5(x,\widehat{s})=0 \tag{25.e}$$

$$-\frac{\partial}{\partial x}\left[\widehat{T}_{SV}+\widehat{T}_W\right]-\frac{\widehat{\mathcal{M}}_Y}{R}-\widehat{q}_6(x,\widehat{s})=0 \tag{25.f}$$

$$\frac{\partial\widehat{B}}{\partial x}-\widehat{T}_W-\widehat{q}_7(x,\widehat{s})=0 \tag{25.g}$$

The equilibrium Eqs. (25) are subjected to the appropriate boundary conditions defined in the Carson domain. Expressions 26.a–26.c represent in the Carson domain the boundary conditions for a clamped end, a free end and a simply supported free-to-warp end, respectively

$$\widehat{u}_{xc}=\widehat{u}_{yc}=\widehat{\theta}_z=\widehat{u}_{zc}=\widehat{\theta}_y=\widehat{\phi}_x=\widehat{\theta}_x=0 \quad \text{at} \quad x=0 \quad \text{or} \quad x=L \tag{26.a}$$

$$\widehat{Q}_X+\frac{\widehat{M}_Z}{R}=\widehat{Q}_Y=\widehat{M}_Z=\widehat{Q}_Z=\widehat{M}_Y-\frac{\widehat{B}}{R}=\widehat{T}_W+\widehat{T}_{SV}=\widehat{B}=0 \quad \text{at} \quad x=0 \quad \text{or} \quad x=L \tag{26.b}$$

$$\widehat{Q}_X+\frac{\widehat{M}_Z}{R}=\widehat{u}_{yc}=\widehat{M}_Z=\widehat{u}_{zc}=\widehat{M}_Y-\frac{\widehat{B}}{R}=\widehat{\phi}_x=\widehat{B}=0 \quad \text{at} \quad x=0 \quad \text{or} \quad x=L \tag{26.c}$$

Consequently, once the boundary conditions are applied, the Eqs. (25) can be solved in the Carson domain considering (22) and (23). Finally, in order to obtain the time response for the problem of linear viscoelasticity, one has to use the inverse Laplace transformation in the solution expressions calculated in the Carson domain employing the following forms:

$$G(t)=O_L^{-1}[\widehat{\mathcal{G}}(\widehat{s})]=O_L^{-1}\left[\frac{\widehat{G}(\widehat{s})}{\widehat{s}}\right] \tag{27}$$

In expression (27), $O_L^{-1}[\bullet]$ is the operator of the inverse Laplace transformation, whereas $\widehat{G}(\widehat{s})$ and $\widehat{\mathcal{G}}(\widehat{s})$ are functions in the Laplace and Carson domains, respectively. The inverse transformation (27) can be performed with either a symbolic or a numerical methodology. The first case is feasible for a quite limited set of configurations, specifically for simple loads and for cross-sections with special orthotropic or symmetric balanced stacking sequences. On the other hand, the second case is more versatile allowing for general loadings and complex stacking sequences.

Although, a symbolic analytical solution of the differential Eqs. (25) in the time domain is completely feasible by means of an algebraic symbolic handling software such as *Mathematica*™ or *MAPLE*™, the advantage is restricted to the cases explained in the previous paragraph and even if it would be possible to solve analytically certain complex problems, it takes a long calculation time (Piovan and Cortínez, 2002). These circumstances compel the employment of a numerical procedure based in the method of finite elements in order to cope with the solution of more general problems related to the linear viscoelastic behavior of thin-walled curved beams.

Note 1: The curved beam model (25) is completely coupled; however it can be decoupled if the conditions of cross-sectional symmetry, at least, in the plane π and special orthotropic or even symmetric balanced laminations are imposed. In these circumstances two subsystems can be decoupled; thus the Eqs.

25.a–25.c represent the In-plane motions (i.e. in the plane π) and Eqs. 25.d–25.g represent the out-of-plane motions. Also under these conditions it is possible to integrate the corresponding equation in order to obtain analytical or closed-form solutions (Piovan, 2003; Piovan and Cortínez, 2005).

Note 2: The model of the curved beam can be reduced to the case of a straight beam if the condition $R \to \infty$ is imposed in equilibrium Eqs. (25) and the related boundary conditions (Piovan, 2003).

Note 3: It is interesting to point out that the Carson transform of a constant is the constant itself as one can deduce from expressions (3) and (27). This simple fact avoids the transformations of many algebraic entities of the model such as, for example, the applied forces among others.

3. Numerical approach based on the method of finite elements

A four-node iso-parametric finite element described in the Carson domain is introduced in this section. The element, denominated ISOP4N, is employed to discretize the spatial domain of thin-walled composite curved beams (Piovan, 2003; Piovan and Cortínez, 2002, 2003b). The interpolation expressions of the generalized displacement in the Carson domain $\widehat{U}_i(\bar{x})$ are given by:

$$\widehat{U}_i(\bar{x}) = \sum_{j=1}^{4} \boldsymbol{f}_j(\bar{x}) \widehat{U}_i^{(j)} \quad \text{with} \quad i = 1, \ldots, 7 \quad \text{and} \quad \bar{x} \in [0,1],\ \bar{x} = \frac{x}{l_e} \tag{28}$$

where, l_e is the length of the element and:

$$\boldsymbol{f}_1(\bar{x}) = 1 - \frac{11}{2}\bar{x} + 9\bar{x}^2 - \frac{9}{2}\bar{x}^3, \quad \boldsymbol{f}_2(\bar{x}) = 9\bar{x} - \frac{45}{2}\bar{x}^2 + \frac{27}{2}\bar{x}^3 \tag{29.a, b}$$

$$\boldsymbol{f}_3(\bar{x}) = -\frac{9}{2}\bar{x} + 18\bar{x}^2 - \frac{27}{2}\bar{x}^3, \quad \boldsymbol{f}_4(\bar{x}) = \bar{x} - \frac{9}{2}\bar{x}^2 + \frac{9}{2}\bar{x}^3 \tag{29.c, d}$$

The vector of nodal displacement of the element can be described in the Carson domain as:

$$\left\{\widehat{U}\right\} = \left\{\left\{\widehat{U}^{(1)}\right\}, \left\{\widehat{U}^{(2)}\right\}, \left\{\widehat{U}^{(3)}\right\}, \left\{\widehat{U}^{(4)}\right\}\right\} \tag{30}$$

where:

$$\left\{\widehat{U}_j^{(i)}\right\} = \left\{\widehat{U}_1^{(i)}, \widehat{U}_2^{(i)}, \widehat{U}_3^{(i)}, \widehat{U}_4^{(i)}, \widehat{U}_5^{(i)}, \widehat{U}_6^{(i)}, \widehat{U}_7^{(i)}\right\}^{\mathrm{T}} = \left\{\widehat{u}_{xc_j}, \widehat{u}_{yc_j}, \widehat{\theta}_{z_j}, \widehat{u}_{zc_j}, \widehat{\theta}_{y_j}, \widehat{\phi}_{x_j}, \widehat{\theta}_{x_j}\right\}^{\mathrm{T}} \tag{31}$$

Now, following the common procedures of the method of finite elements (Oñate, 1992; Zienkiewicz, 1980) but here drawn in the Carson domain, one arrives to:

$$\left|\widehat{\boldsymbol{K}}\right|\left\{\widehat{\boldsymbol{W}}\right\} = \left\{\widehat{\boldsymbol{P}}\right\} \tag{32}$$

where $\left|\widehat{\boldsymbol{K}}\right|$ is the global stiffness matrix in the Carson domain, whereas $\left\{\widehat{\boldsymbol{W}}\right\}$ and $\left\{\widehat{\boldsymbol{P}}\right\}$ are the global vector of nodal displacements in the Carson domain and the global vector of nodal loads in the Carson domain, respectively. A scheme of reduced integration (Oñate, 1992) is employed to avoid the shear-locking phenomenon.

The numerical calculation scheme for the structural response of linear viscoelastic composite thin-walled curved beams can be observed in Fig. 3. The first steps correspond to the definition of the micro and macromechanics of the laminates, and the adoption of the structural model (curved or straight beam) and its main characteristics (shear deformable or non-shear deformable). The finite element method is employed to discretize the spatial domain of the beam. Note that in this article four-node isoparametric elements are employed, however the calculation scheme can be also suitable for other types of elements (Piovan and Cortínez, 2002, 2003b). Then for each node, a set of N_L values of the Carson variable $\widehat{s}$ is adopted, and for each value of $\widehat{s}$ the structural response (node displacements, strains, etc.) is obtained. In these circumstances one has at each node and element the viscoelastic behavior posed numerically in the Carson domain. At this point one may invert

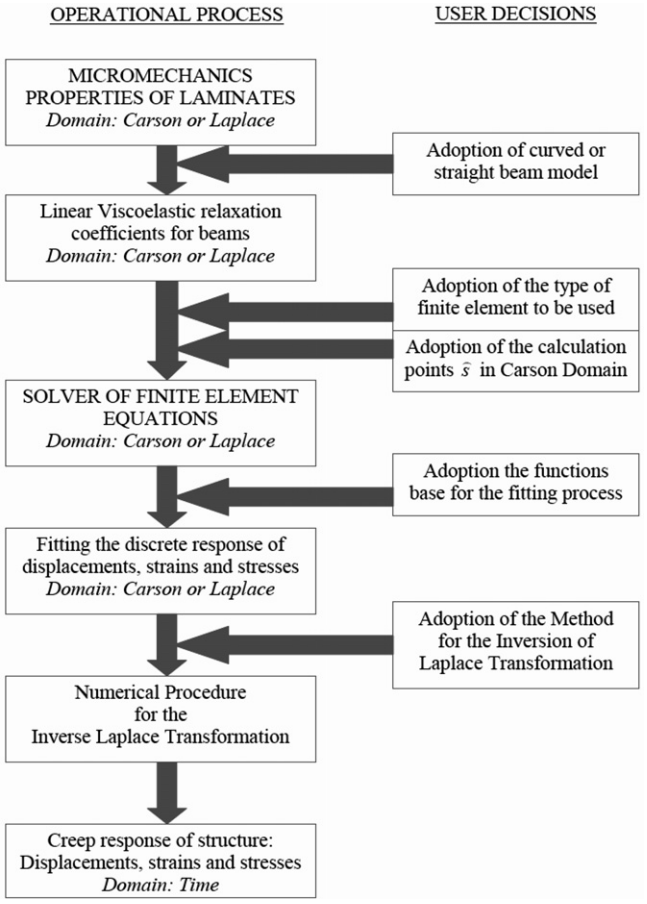

Fig. 3. Calculation flowchart.

the response in a given point posed in Carson domain in order to obtain the response in time domain. This can be done by means of two different schemes. The first scheme implies the numerical inversion of the response posed in the Carson domain arriving to a discrete response in the time domain, i.e. a set of values in the instants t_0, t_1, t_2, etc. that may be fitted with a certain set of power-law functions in order to reach to the continuous creep response (Qiao et al., 2000; Barbero, 2007). The second scheme is the one employed in the present paper. Thus, a set of functions $\mathcal{P}_j(\widehat{s})$, $j = 1,2,3,\ldots,\infty$, is selected to fit the discrete responses of a given displacement posed in the Carson domain leading to a continuous expression in the variable $\widehat{s}$. Finally the continuous response in the Carson domain is transformed into the time-domain by means of a numerical procedure of the Laplace inverse transformation such as Stehfest method or Piessens method or Durbin method or Weeks method or Crump method, etc., as one can see in Mallet (2002). The set of fitting functions (33) can be employed in order to obtain the algebraic expressions in the Carson domain. These functions proved to reach very good performance when compared with the available analytical solutions (Piovan and Cortínez, 2002; Cortínez and Piovan, 2001).

$$\mathcal{P}_j(\widehat{s}) = \widehat{s}^{-1/j}, \quad \text{with} \quad j = \{1,2,3,4,5,6,\ldots,\infty\} \tag{33}$$

Normally, one requires just a few fitting functions (33) and models with a few finite elements to reach good results and good approximations. The set of functions (33) are one of the sets that may be employed in the linear and nonlinear fit procedures that offers the software *Mathematica*™ (Wolfram, 1999).

The calculation scheme of the present approach is programmed in the software *Mathematica*™ which provides the context for doing numerical or symbolic analysis in the same environment. Thus, with this scheme

one can obtain in a unified fashion analytical solutions (in the cases where it is possible) as well as numerical approximations of the creep behavior.

4. Examples on the linear viscoelasticity of thin-walled beams

4.1. Validation of the linear elastic structural model

It is important to show examples of the validity of the linear elastic structural model employed. Take into account that the general structural model employed in the present paper is a thin-walled curved beam for static purposes which can be reduced (by means of $R \to \infty$) to a thin-walled straight beam model.

The first example corresponds to a curved I-beam with the following geometric properties: radius $R = 1$ m, Length $L = 3$ m, web height $h = 0.1$ m, flange width $b = 0.1$, laminate thickness $e = 0.005$ m. The web is perpendicular to the curvature radius. Flanges and web have the following stacking sequences $\{0/\pm 45/90\}_S$ or $\{0/0/\pm 45\}_S$. The material is such that $E_1 = 144$ GPa, $E_2 = 9.68$ GPa, $G_{12} = G_{13} = 4.14$ GPa, $G_{23} = 3.45$ GPa, $v_{12} = 0.3$, $v_{23} = 0.5$. The curved beam is clamped at both ends and an out-of-plane flexural load of $Q_Z = 10$ N is applied at $x = L/2$. In Fig. 4 one can see a comparison between the curved beam model (Piovan and Cortínez, 2007b) and a computational finite element approach performed with shell elements of the Commercial Program Cosmos/M. The shell models were prepared with more than 3000 SHELL8T finite elements whereas the response of the one-dimensional model was performed with four curved finite elements. As one can see, the correlation of one-dimensional approach and shell approach is quite good. In these cases differences of less than 2.5% have been reached between the shell and beam approaches. In a recent work of the authors (Piovan and Cortínez, 2007b) one can find extensive comparisons of the thin-walled curved beam model for composite materials, in different linear elastic problems (static, vibration and buckling).

The second example is a comparison of different straight thin-walled beam models for composite materials. It consists of three different cases of closed box beam clamped at $x = 0$ and subjected to a certain load at $x = L$. The length of the beam is 0.762 m the cross-section is such that it has a panel thickness of 0.762 mm, with web height of 12.84 mm and flange width of 23.44 mm. The width and height are measured between the mid-lines of the wall thickness. In the first case, the beam has a circumferentially uniform stiffness (CUS) lay-up of $\{15\}_6$ and the beam is subjected to a flexural load of $Q_Z = 4.45$ N at $x = L$ and directed towards the web direction. The lay-up of the second and third is a circumferentially asymmetric stiffness (CAS) of $\{45\}_6$, $\{-45\}_6$, $\{45/-45\}_3$ and $\{-45/45\}_3$ in top flange, bottom flange, right web and left web, respectively. The loads applied at $x = L$, in the second and third cases are a flexural load of $Q_Z = 4.45$ N and a twisting moment of $M_X = 0.113$ Nm, respectively. The elastic material properties are such that $E_1 = 141.96$ GPa, $E_2 = 9.79$ GPa, $G_{12} = G_{13} = 6.01$ GPa, $G_{23} = 4.83$ GPa, $v_{12} = 0.24$, $v_{23} = 0.5$. For other complementary details one can see the works of Kim and White (1997) and Smith and Chopra (1991). In

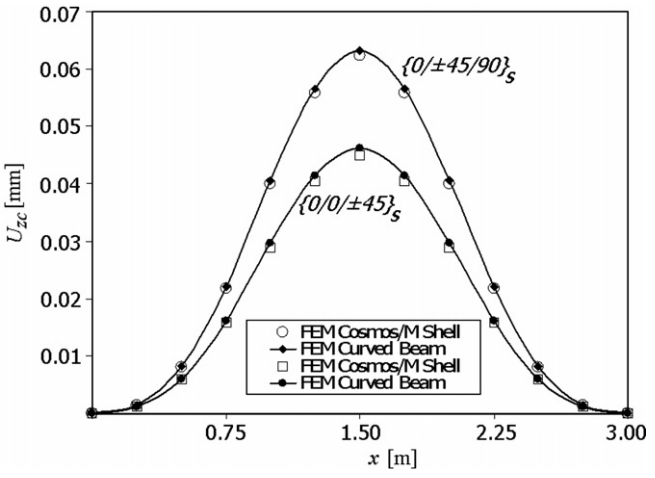

Fig. 4. Out-of-plane bending displacement of a clamped curved beam: comparison of shell and beam approaches.

Fig. 5(a) one can see the bending slope of different thin-walled straight beam models. In Fig. 5(b) one can see the twisting angle due to elastic couplings related to a flexural force. On the other hand, in Fig. 5(c) one can see the bending slope due to elastic couplings connected with a twisting moment.

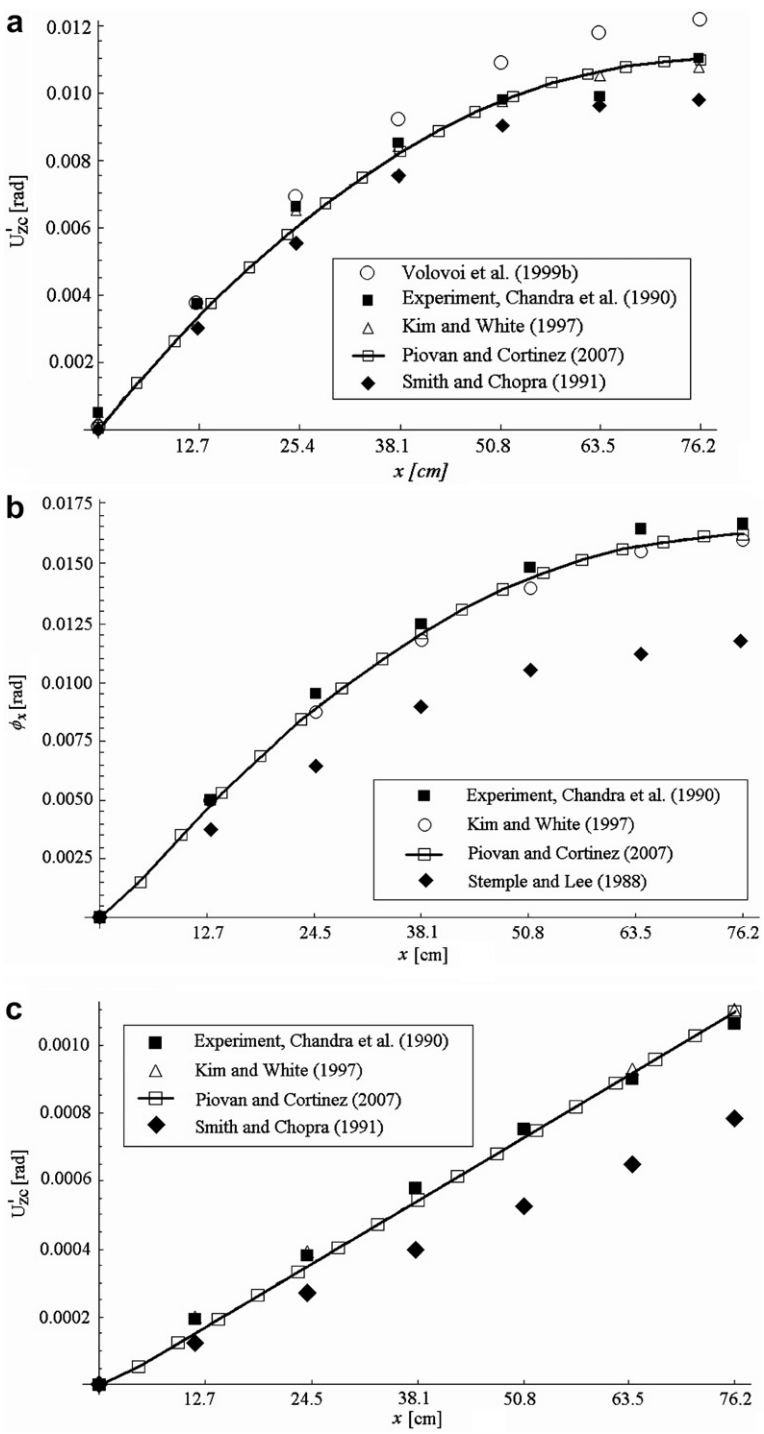

Fig. 5. Comparison of different beam models. (a) Bending slope of a cantilever straight beam under flexural load. (b) Twisting angle of a cantilever beam under flexural load. (c) Bending slope of a cantilever straight beam under torsional load. (See above-mentioned references for further information.)

In a recent work of the authors (Piovan and Cortínez, 2007a) one can find many other comparisons and validations of the thin-walled straight beam model (reduced from the curved beam model) for composite materials, in different linear elastic problems such as free vibrations with or without initial stresses, buckling and general static problems.

4.2. Convergence and comparisons

In order to check the numerical methodology for the viscoelastic analysis a few convergence tests are performed. The first test considers a straight (i.e. $R \to \infty$) cantilever box-beam with a cross-section of height $h = 0.20$ m, width $b = 0.10$ m and a wall thickness of $e = 0.01$ m, and the beam is such that $h/L = 0.05$. The stacking sequence of each panel is {0/0/0/0} and the properties of the material can be found in Table 1 with a fiber volume fraction $V_F = 0.54$. The linear viscoelastic behavior of the plastic matrix can be represented with the four-parameters Maxwell–Voigt model. A bending force of $Q_Z = 500$ N is applied at $x = L$ in the direction of the larger panels. Under these circumstances, the bending deflection at the free end can be described analytically. The analytical expression for the bending deflection at the free end in the Carson domain is given by the following form:

$$\widehat{U}_{zc} = \frac{Q_Z L^3}{3\widehat{\overline{J}}^{11}_{22}} + \frac{Q_Z L}{\widehat{\overline{J}}^{66}_{66}} \tag{34}$$

A finite element model with four ISOP4N elements is employed to perform the computation on a set of 30 locations of the Carson domain variable $\widehat{s}$. The 30 discrete values of $\widehat{U}_{zc}$ were adjusted with three different sets of 15, 10 and 5 fitting functions which are shown in expression (35). The numerical inversion of the Laplace transform is performed with the Stehfest method (Mallet, 2002), which has proved to be computationally faster than the others (Piovan and Cortínez, 2002, 2003b).

$$\mathcal{D}(\widehat{s}) = \left\{1, \widehat{s}^{-1}, \widehat{s}^{-0.9}, \widehat{s}^{-0.8}, \widehat{s}^{-0.7}, \widehat{s}^{-0.6}, \widehat{s}^{-0.5}, \widehat{s}^{-0.4}, \widehat{s}^{-0.3}, \widehat{s}^{-0.2}, \widehat{s}^{-0.1}, \widehat{s}^{-0.05}, \widehat{s}^{-0.02}, \widehat{s}^{-0.01}, \widehat{s}^{-0.005}, \widehat{s}^{-0.001}\right\} \tag{35.a}$$

$$\mathcal{D}(\widehat{s}) = \left\{1, \widehat{s}^{-1}, \widehat{s}^{-0.8}, \widehat{s}^{-0.7}, \widehat{s}^{-0.6}, \widehat{s}^{-0.5}, \widehat{s}^{-0.4}, \widehat{s}^{-0.3}, \widehat{s}^{-0.2}, \widehat{s}^{-0.1}\right\} \tag{35.b}$$

$$\mathcal{D}(\widehat{s}) = \left\{1, \widehat{s}^{-1}, \widehat{s}^{-0.5}, \widehat{s}^{-0.3}, \widehat{s}^{-0.1}\right\} \tag{35.c}$$

In Fig. 6, one can see the comparison of the analytical solution and finite element approximations in the time domain of the creep response. Note that in this case, 10 fitting functions are good enough to reach an acceptable matching with the analytical solution. Fig. 7 shows, for the same previous example, a convergence of the finite element employed. Note that one element is enough to reach a very good approximation.

As it was told in the Note 1 of Paragraph 2.2, under certain conditions it is possible to obtain closed-form solutions for the in-plane or out-of-plane motions of the curved beam model. Thus, for a cantilever curved box-beam with symmetric cross-ply lamination {0/90/90/0}, with a subtended angle of $\pi/2$, and with a uniformly distributed radial load q_y, the radial displacement u_{yc} is obtained from the closed-form solutions given in reference (Piovan and Cortínez, 2005) and it can be described in the Carson domain according to the following form:

$$\widehat{U}_{yc} = \frac{q_y R^2}{2}\left(\frac{1}{\widehat{\overline{J}}^{11}_{11}} + \frac{1}{\widehat{\overline{J}}^{66}_{55}} + \frac{R^2}{\widehat{\overline{J}}^{11}_{33}}\right) \tag{36}$$

Table 1
Properties of glass fibers and for the four-parameter model of an ED-6 matrix

$E_F = 68.67$ GPa,	$v_F = 0.21$, $v_M = 0.38$,
$E^{(e)} = 3.27$ GPa,	$\eta^{(M)} = 8000$ GPa h
$E^{(V)} = 1.80$ GPa,	$\eta^{(V)} = 300$ GPa h

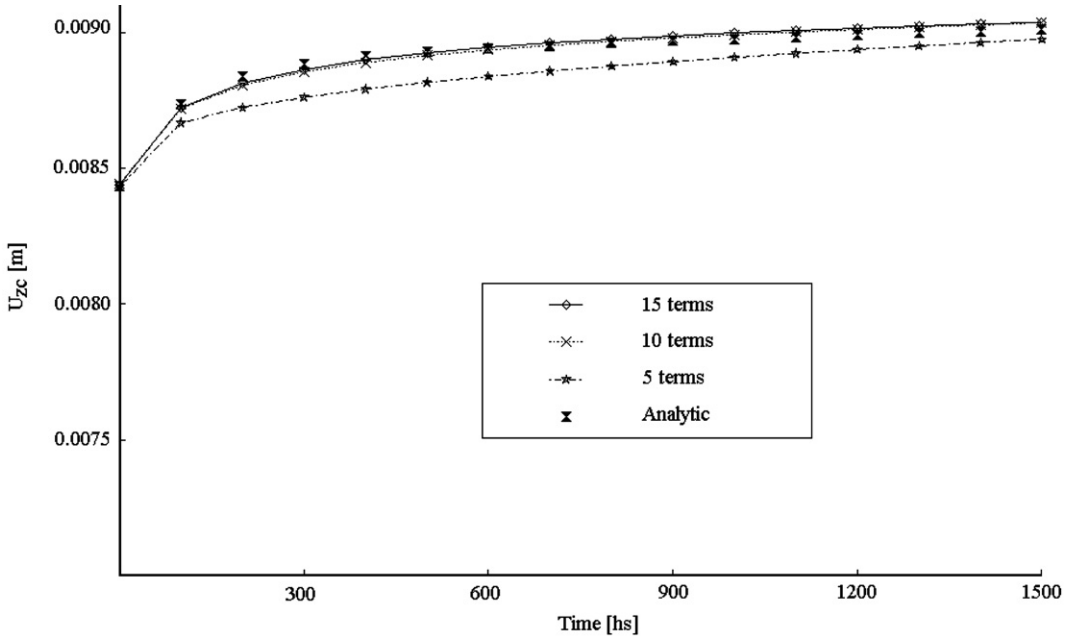

Fig. 6. Bending displacement of a cantilever straight beam: comparison of adjustment functions.

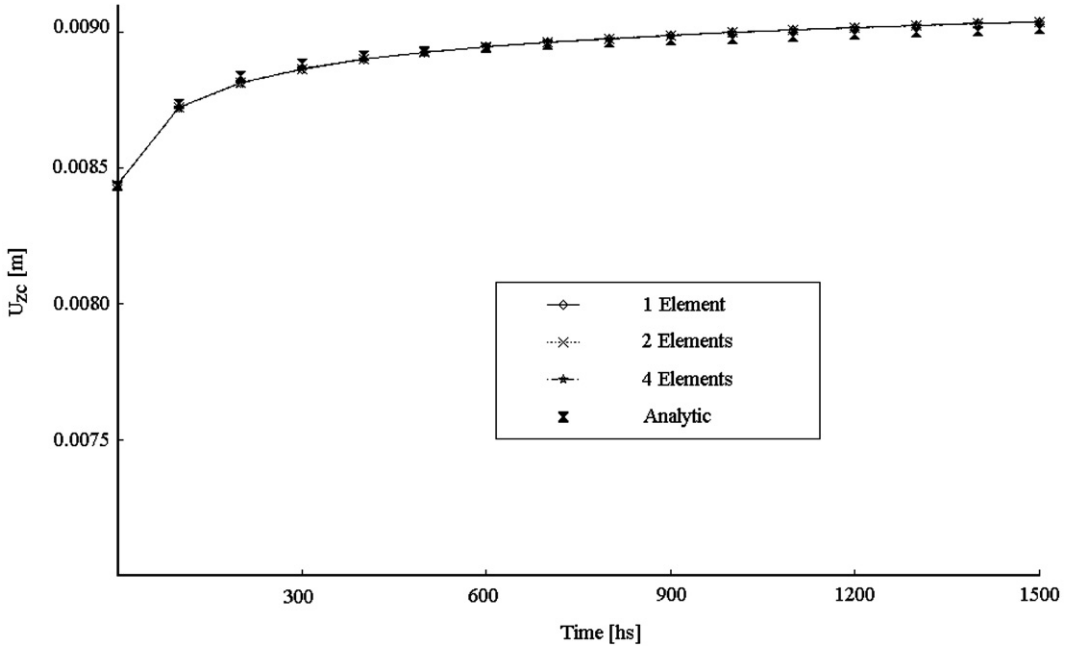

Fig. 7. Bending displacement of a cantilever straight beam: convergence test.

In Fig. 8, one can see a convergence test of the finite element approximations for the creep behavior of the radial displacement under a constant distributed load of $q_y = 50$ N/m. The curved beam has a squared cross-section with a side of $h = 0.05$ m. (measured at the midline of the wall thickness); the wall thickness and the curvature radius are such that $e/h = 0.1$ and $h/R = 0.05$. The beam is constructed with the material whose properties are shown in Table 1 with a fiber volume fraction $V_F = 0.54$. Finite element models of

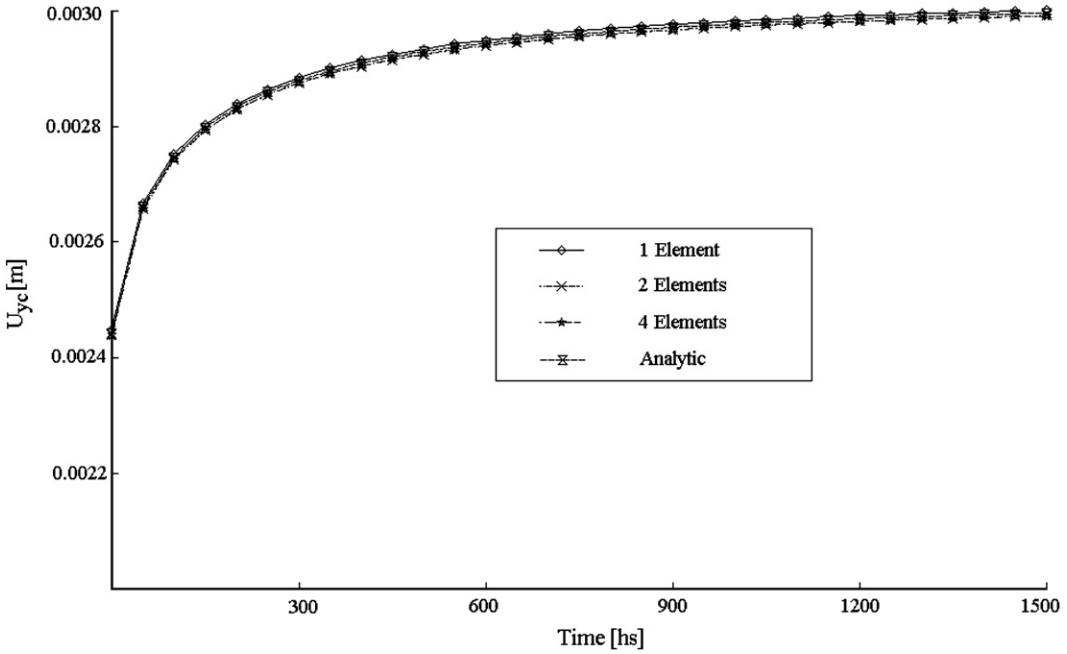

Fig. 8. In-plane bending displacement of a cantilever curved beam: convergence test.

one, two and four ISOP4N elements are employed to perform the computation on a set of 30 locations $\widehat{s}$ of the Carson domain. These 30 discrete values of U_{yc} were fitted with the base of fifteen fitting functions given in expression (35.a), and the Stehfest method (Mallet, 2002) was employed to perform numerically the inverse Laplace transformation. In Fig. 8 it is possible to see a good convergence to the analytic solution, even with one element there is a maximum relative error with respect to the analytic solution of about 0.2%.

4.3. Comparisons with experimental data and other approaches

The creep response of a unidirectional FRP specimen whose properties are those of Table 1 with $V_F = 0.54$ is shown in Fig. 9. The axial compliance coefficient (namely $\varepsilon(t)/\sigma$) of the specimen can be obtained by inverting the transversely isotropic relaxation tensor (11). The numerical approach of the compliance coefficient correlates quite well with the experimental data available (Luciano and Barbero, 1995) for three different levels of applied stress during a 12:00-h period.

Fig. 10 shows the compliance coefficient of a Derakane 411-350 resin. The experimental data has been taken from the work of Harris and Barbero (1998) that employed a two-parameter Maxwell model to represent the creep behavior during a 4-h period. On the other hand the authors of the present paper employed a non-linear fitting procedure in order to fit the aforementioned experimental data to a four-parameter Maxwell–Voigt model. The viscoelastic properties of this material are shown in Table 2. The Maxwell model and the Maxwell–Voigt model were employed to evaluate the compliance coefficient of a $\{[90/45/-45/\mathrm{CSM}]_3\}_S$ laminate with $V_F = 0.44$. Fig. 11 shows the variation of the axial compliance coefficient. As one can see the present numerical procedure with both the two-parameter and four-parameter models agrees very well with the available experimental data during a 22-h period.

The creep behavior under bending loading of a glass fiber-reinforced-plastic straight box-beam is analyzed. The pultruded box-beam was tested experimentally by Qiao et al. (2000), who also developed a beam model for the analysis of linear viscoelasticity. The box-beam is simply supported with a length of 3.66 m, and the cross-section of $101.6 \times 101.6 \times 6.35$ mm (measured in the outer surfaces, not in the middle line of the wall) is manufactured with E-glass fiber and vinylester resin with the properties shown in Table 3 (the plastic matrix is supposed to respond to a two-parameter Maxwell model), and each panel has a stacking sequence of three

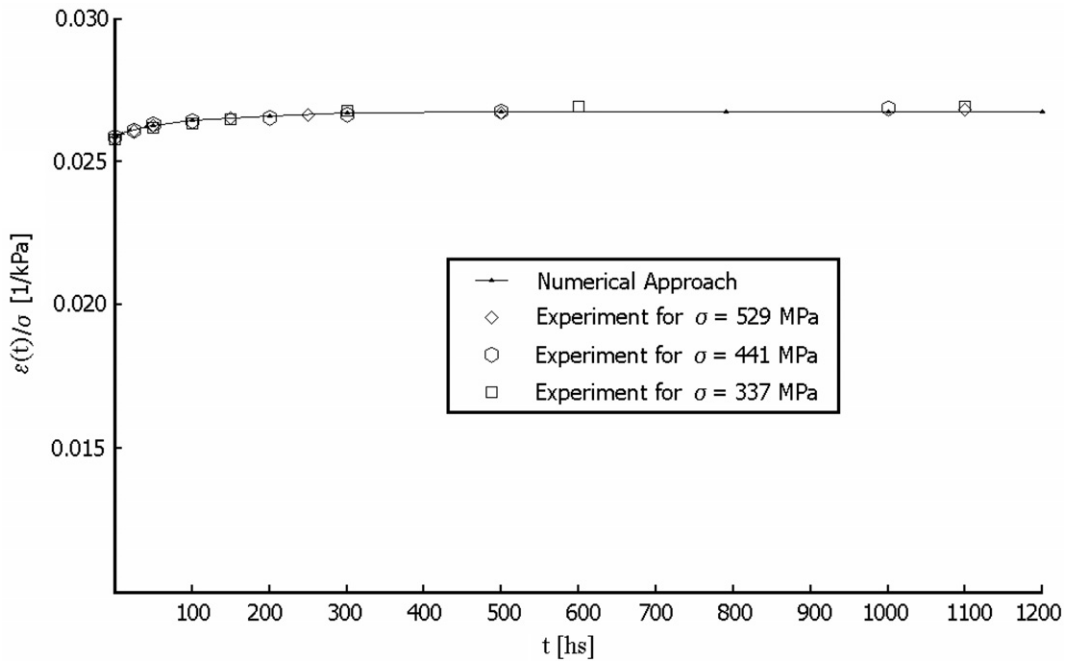

Fig. 9. Variation of compliance coefficient of an ED-6 resin matrix specimen under constant tensile stress. Comparison of the present numerical approach with the available experimental data.

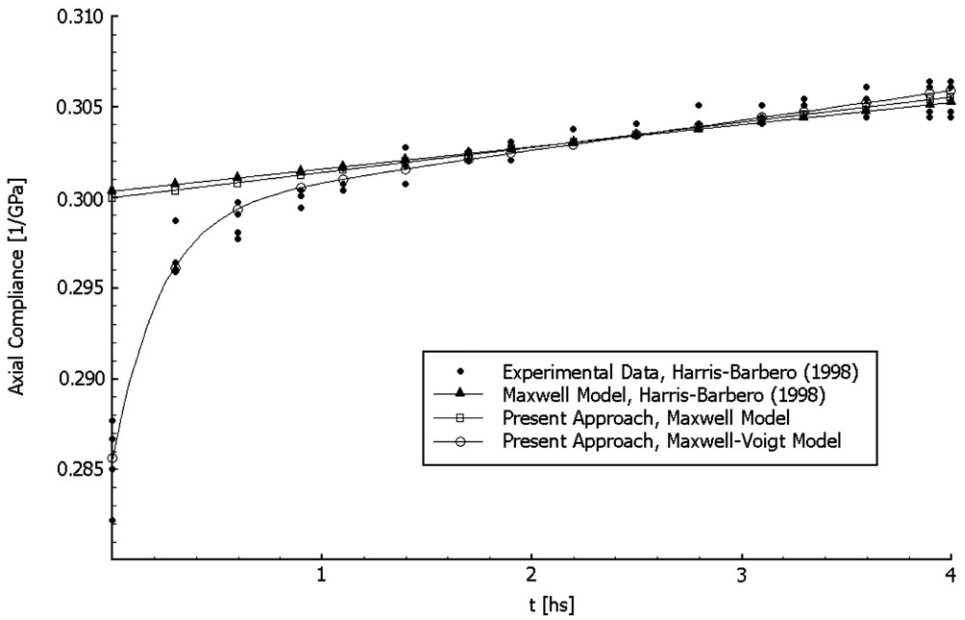

Fig. 10. Variation of the compliance coefficient for a Derakane 411-350 matrix. Comparison of Maxwell models with the available experimental data.

layers: the outer of unidirectional roving and the other two of continuous strand mats (CSM). The beam is subjected to loads of 4500 N applied at $x = 1/3L$ and $x = 2/3L$ during a period of 120 h. In order to compare the present methodology with other approaches, the linear viscoelastic behavior of the vinylester matrix was modeled with the Maxwell model (5). A model of five ISOP4N finite elements, a set of 25 discrete locations $\widehat{s}$

Table 2
Properties of E-glass fibers and for the Maxwell models of a Derakane 411-350 matrix

$E_F = 72.5$ GPa, $v_F = 0.22$
Two-parameter Maxwell model
$E^{(M)} = 3.33$GPa
$\eta^{(M)} = 854.6$ GPa h, $v_M = 0.38$
Four-parameter Maxwell model
$E^{(e)} = 3.58$ GPa, $\eta^{(M)} = 608$ GPa h
$E^{(V)} = 72.5$ GPa, $\eta^{(V)} = 16.1$ GPa h, $v_M = 0.38$

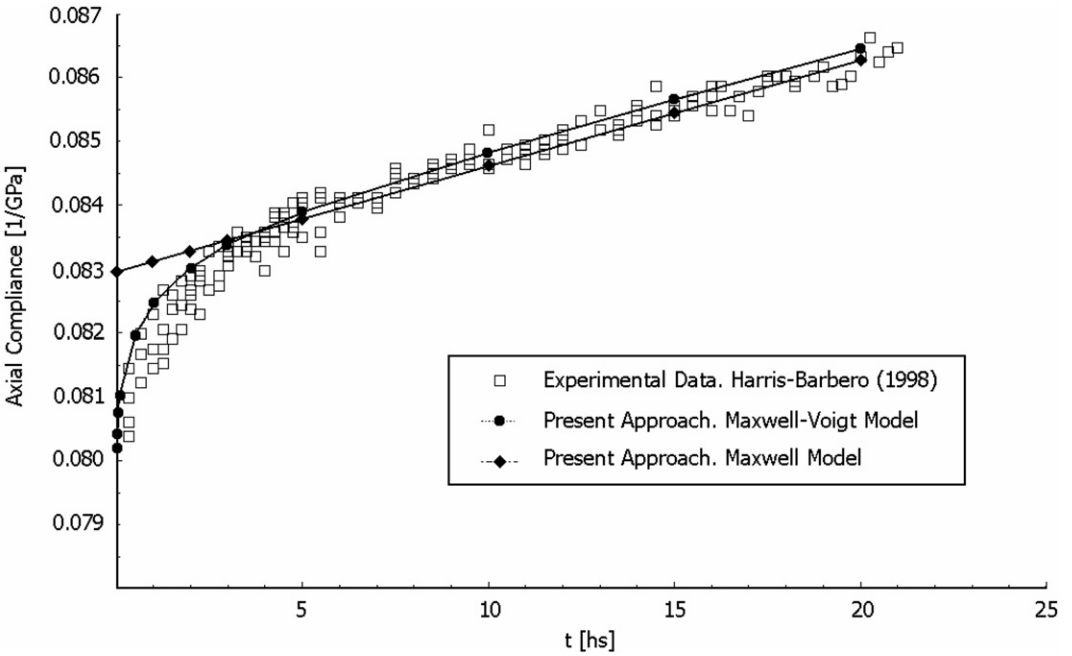

Fig. 11. Variation of compliance coefficient of the laminate $\{[90/45/-45/\mathrm{CSM}]_3\}_S$ under constant tensile stress. Comparison of the present numerical approach with the available experimental data.

Table 3
Properties of E-glass fibers and for the two-parameter model of a Vinylester matrix

$E_F = 72.5$ GPa, $v_F = 0.22$,
$E^{(M)} = 3.86$ GPa, $\eta^{(M)} = 855.09$ GPa h, $v_M = 0.38$

in the Carson domain and a set of 12 fitting functions were employed to perform the calculations with the present approach. The Stehfest method (Mallet, 2002) for the numerical inversion of Laplace transform is employed. Fig. 12 shows, for the mid-span deflection, a comparison of the experimental results and model predictions of Qiao et al. (2000) and the predictions of the present finite element approach. In Fig. 12, one can see that differences between model predictions and experimental responses are less than 3.0% during a five-day period. It is important to take into account that, although in this example the structural model employed by Qiao et al. (2000) and the authors (i.e. the case reduced to a straight beam) is practically the same, i.e. a Timosheko bending model, however there are differences between the calculation methodology employed in the present approach and the one used by Qiao et al. (2000). Effectively, Qiao et al. employed a collocation

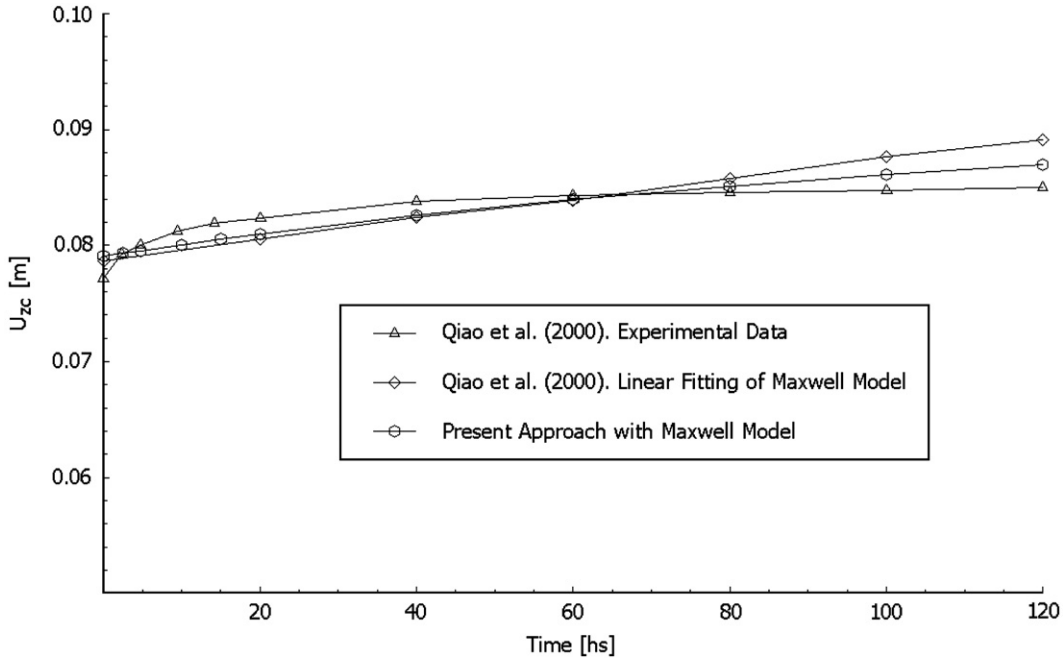

Fig. 12. Mid-span bending displacement of the box-beam. Comparison of models and experiments.

method to perform the inverse Laplace transformation obtaining discrete values in the time domain and then adjusting the solution in the time domain, whereas in the present approach the responses in discrete locations of the Carson domain are adjusted with a given base as a previous step to the numerical inversion of the Laplace transformation. As it was mentioned previously, one can obtain in a unified fashion analytical solutions as well as numerical approximations.

Now, the creep behavior under bending loading of a pultruded straight I-beam is analyzed. A cross-section with 0.3048 m of flange width and web height (measured in the outer surfaces), and a thickness of 0.0127 m, is employed. The three panels have the same lay-up composed by 13 plies in the following configuration $\{(a/b)_6/a/(b/a)_6\}$; where 'b' corresponds to 54 roving layers, and 'a' corresponds to a combination of continuous strand mat (5%) and stitched fabrics (13%) with angular orientation (for particular details see Qiao et al., 2000). The material viscoelastic properties are the ones of Table 3. The beam is simply supported, with a length $L = 3.66$ m. and subjected to a central load of $Q_Z = 4500$ N. whose direction is parallel to the web. In Fig. 13 one can see a comparison between the present approach (i.e. the reduced case of straight beam) and the approach of Qiao et al. (2000) of the linear viscoelastic behavior of the mid-span displacement for a beam with stitched fabrics oriented along the beam axis and for two different fiber volume fractions. During the analyzed period of 400 h, both approaches correlate quite well.

4.4. Linear viscoelastic behavior of thin-walled curved beams with open section

In Fig. 14(a) the dimensions of the cross-section of a curved beam are presented. The curved beam has a length of $L = 1.5$ m, a curvature radius of $R = 2$ m, it is clamped at $x = 0$ and free at $x = L$ where the forces $Q_Y = 500$ N and $Q_Z = 500$ N are applied in the point $\boldsymbol{C}$. The panels are constructed with the material whose properties are shown in Table 1 with a fiber volume fraction $V_F = 0.54$. Each panel has a stacking sequence $\{0/0/-\alpha/\alpha\}_S$, that is a symmetric balanced lamination. In Fig. 15 one can see the variation of the relaxation coefficient $\overline{A}_{11}$ for three different laminates employed in the open section beam. This kind of stacking sequence does not produce constitutive elastic couplings, then Q_Y leads only to in-plane bending motions and Q_Z leads to a coupled out-of-plane bending-twisting motion, due to mono-symmetry of the cross-section. In Figs. 16–18 one can see the creep behavior for different fiber orientation of $u_{yc}(L)$, $u_{zc}(L)$ and $\phi_x(L)$, respectively. Note that the secondary creep tends to stabilize beyond 800 h in many cases. Note in Fig. 17 that the creep behavior of

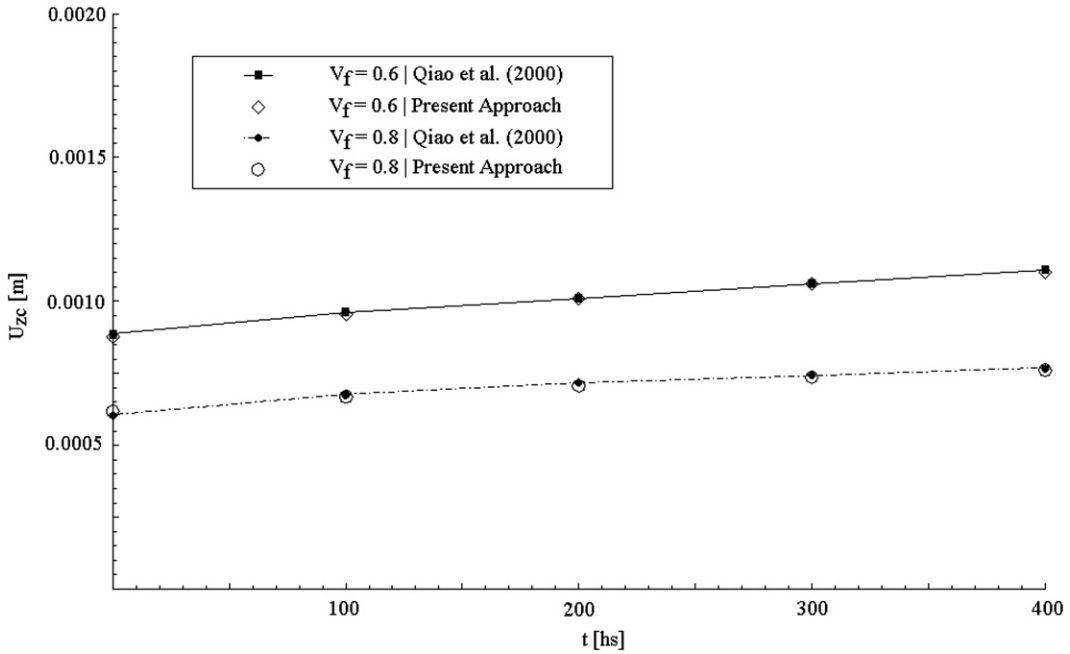

Fig. 13. Mid-span displacement of a simply supported straight beam under central load: comparison of viscoelastic results of different authors.

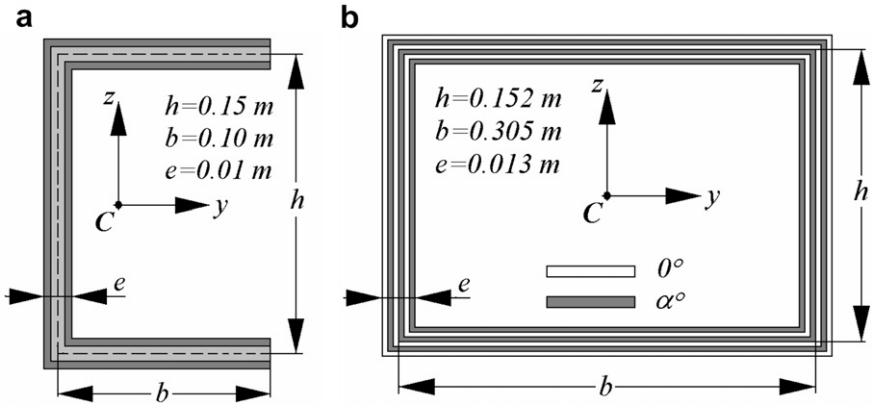

Fig. 14. Dimensions and stacking sequence of (a) U-profile. (b) Closed rectangular section.

displacement $u_{zc}(L)$ has the best performance for $\alpha = 15°$, i.e. with the least deflections and with lower deflection gap since the forces are acting. This deflection gap can be calculated by means of the ratio of $u_{zc}(L)|_{t=1200}$ with respect to $u_{zc}(L)|_t = 0$. In the cases of $\alpha = 15°$ and $\alpha = 0°$, the deflection gap reach values of 34% and 51%, respectively. In Figs. 19 and 20 one can see the variation, with respect to the angle of fiber reinforcement, of $u_{zc}(L)$ and $\phi_x(L)$ for different instants. Note that the stacking sequence case with $\alpha = 15°$ has the best performance (meaning the minimum deflection) in both variables.

4.5. Linear viscoelastic behavior of thin-walled curved beams with closed section

Fig. 14(b) shows the dimensions of a closed cross-section with stacking sequence of $\{(0/\alpha)_3\}$. This kind of lamination is denominated circumferentially uniform stiffness (CUS) and it is such that provides a selective

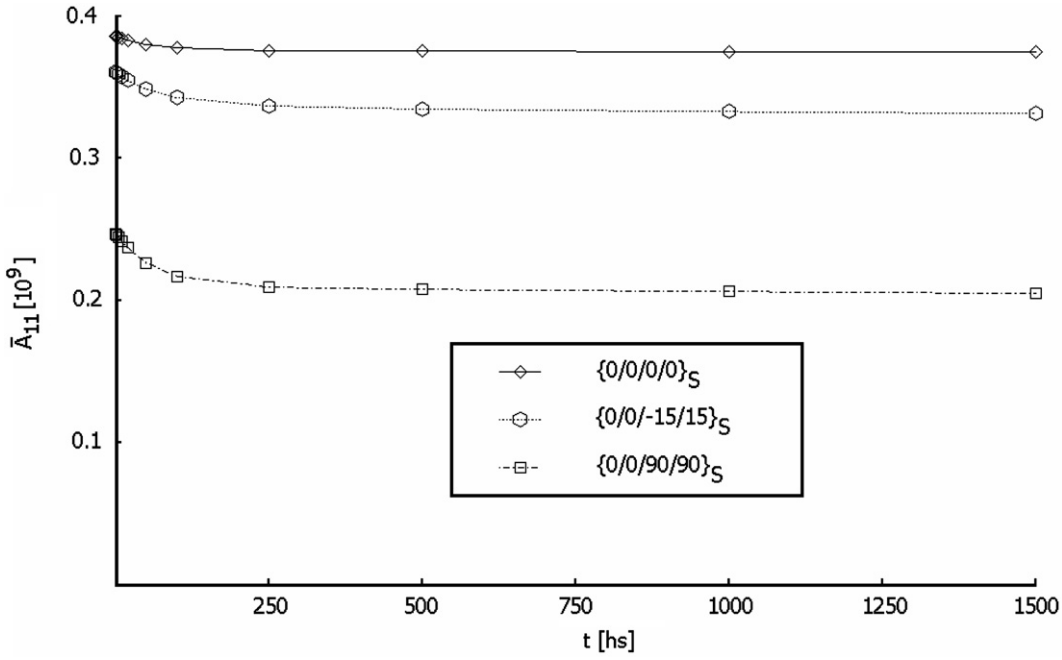

Fig. 15. Variation of the relaxation coefficient $\bar{A}_{11}$ for three different laminates employed in the curved U-beam.

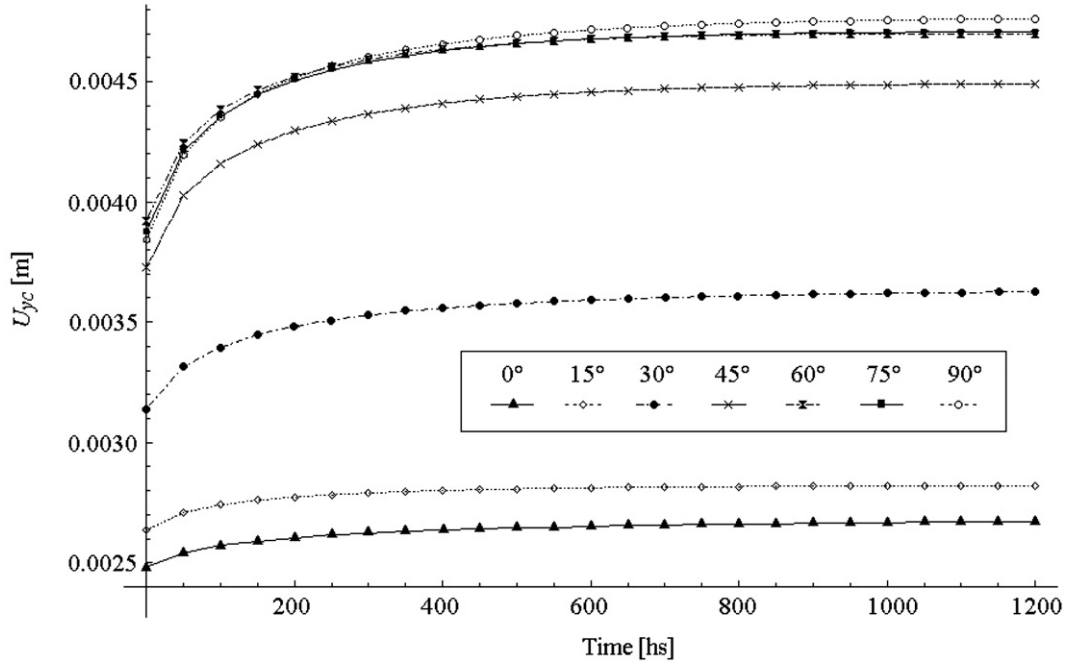

Fig. 16. Creep displacement $u_{yc}(L)$ under an in-plane bending load, for a U-profile.

elastic coupling between in-plane and out-of-plane motions. In Fig. 21 one can see the variation of the relaxation coefficient $\overline{A}_{11}$ (see Piovan and Cortínez, 2007a; for definitions) for three different laminates employed in the closed section curved beam. The beam is clamped at both ends and it is constructed with a material of Table 1 with a fiber volume fraction $V_F = 0.54$, $R = 2.546$ m and the subtended angle is $\beta = 90°$. The stacking

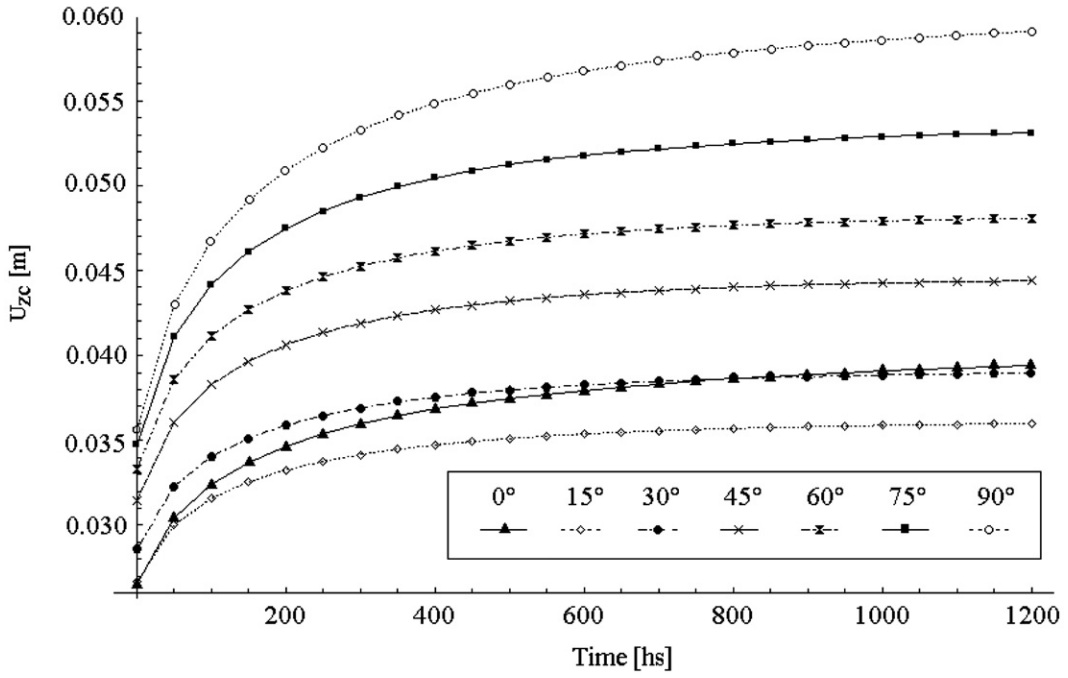

Fig. 17. Creep displacement $u_{zc}(L)$ under an out-of-plane bending load, for a U-profile.

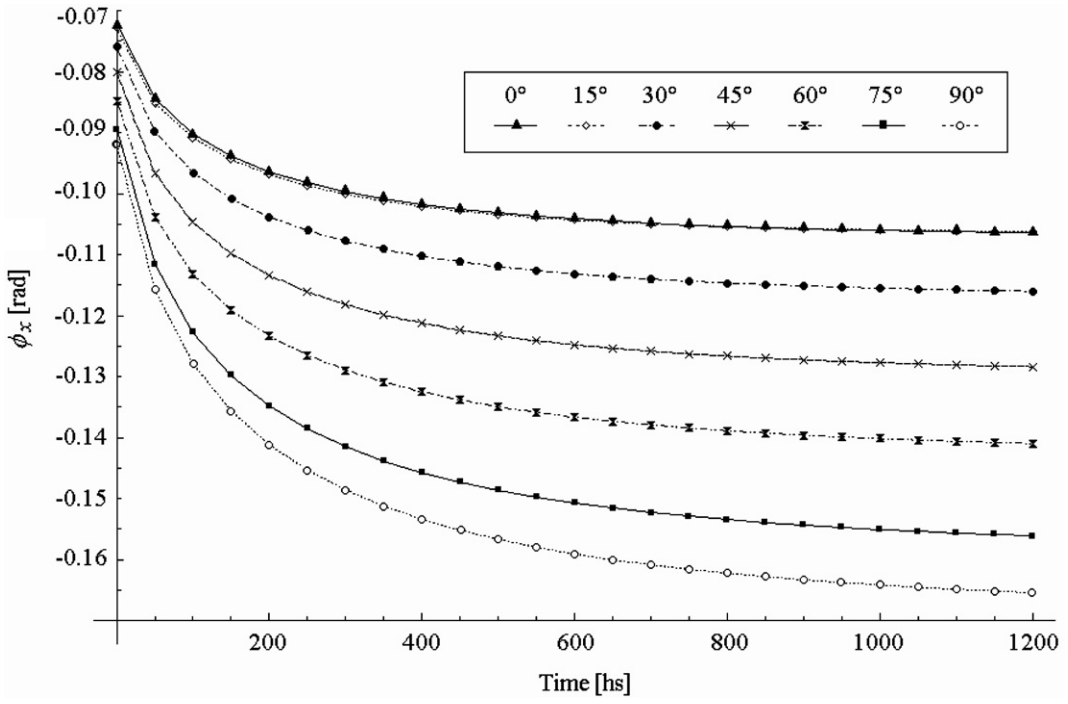

Fig. 18. Twisting angle $\phi_x(L)$ under an out-of-plane bending load, for a U-profile.

sequence of the panels corresponds to a type denominated "Circumferentially Uniform Stiffness" or CUS that leads to a constitutive elastic coupling between twisting and extension motions and bending-bending motions.

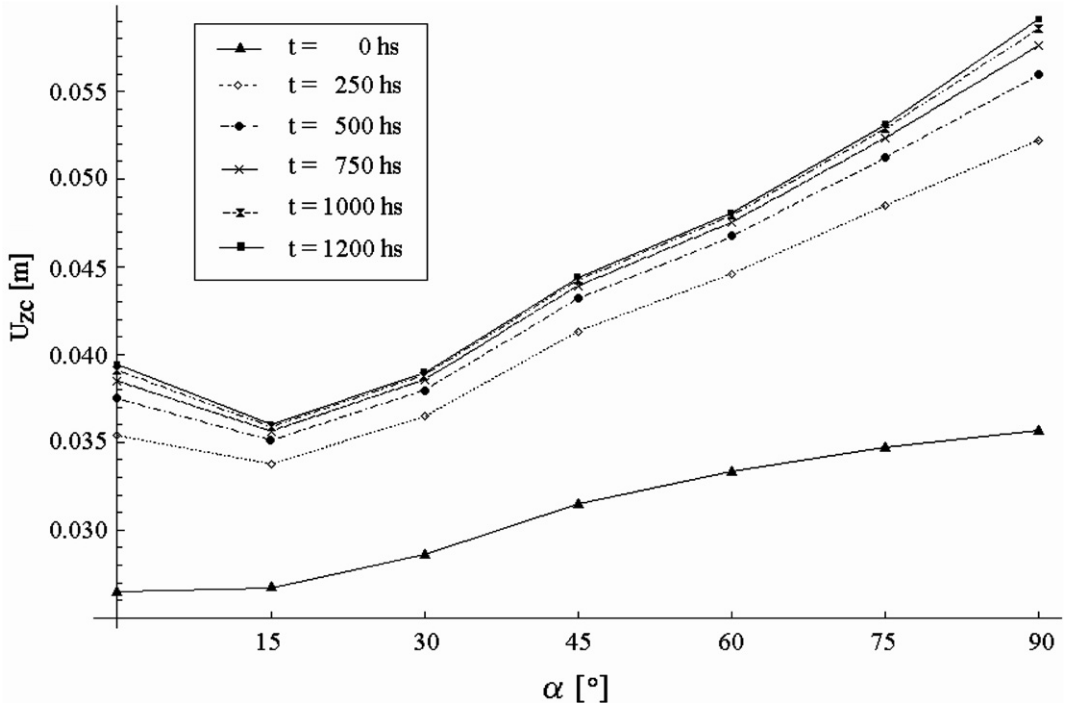

Fig. 19. Variation of $u_{zc}(L)$ with respect to the fiber orientation angle, for a U-profile.

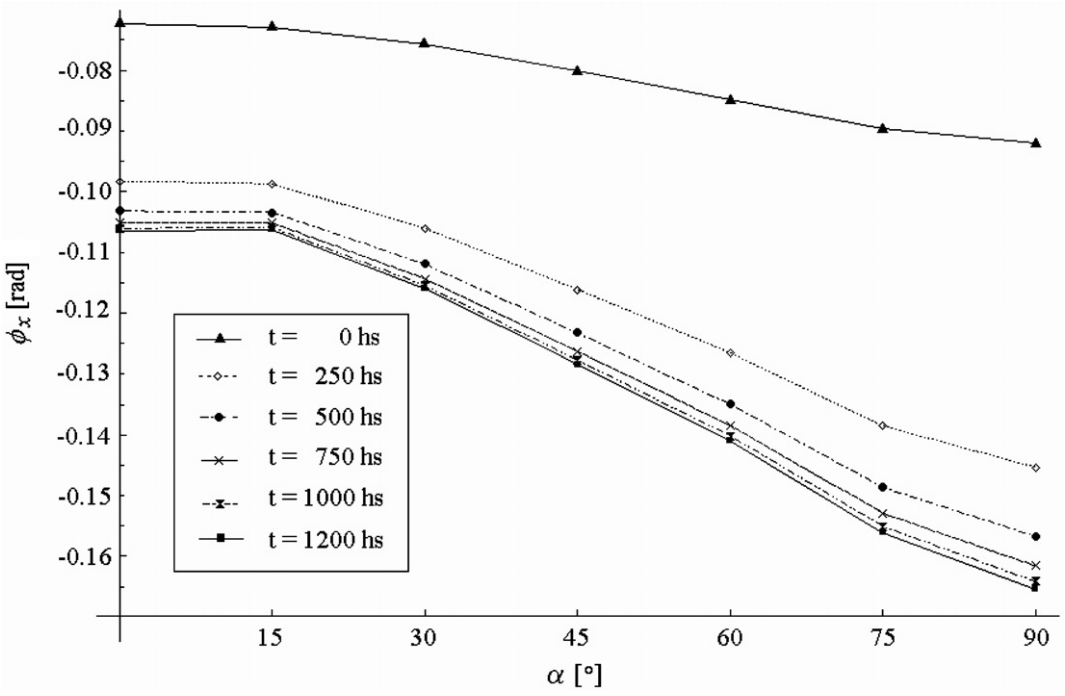

Fig. 20. Variation of $\phi_x(L)$ with respect to the fiber orientation angle, for a U-profile.

Under these conditions, the out-of-plane loading induces in-plane displacements. The curved beam is subjected to an out-of-plane bending force $Q_Z = 4500$ N and a total twisting moment $M_X = 4000$ Nm that are applied in the point $\boldsymbol{C}$ located at $x = L/2$.

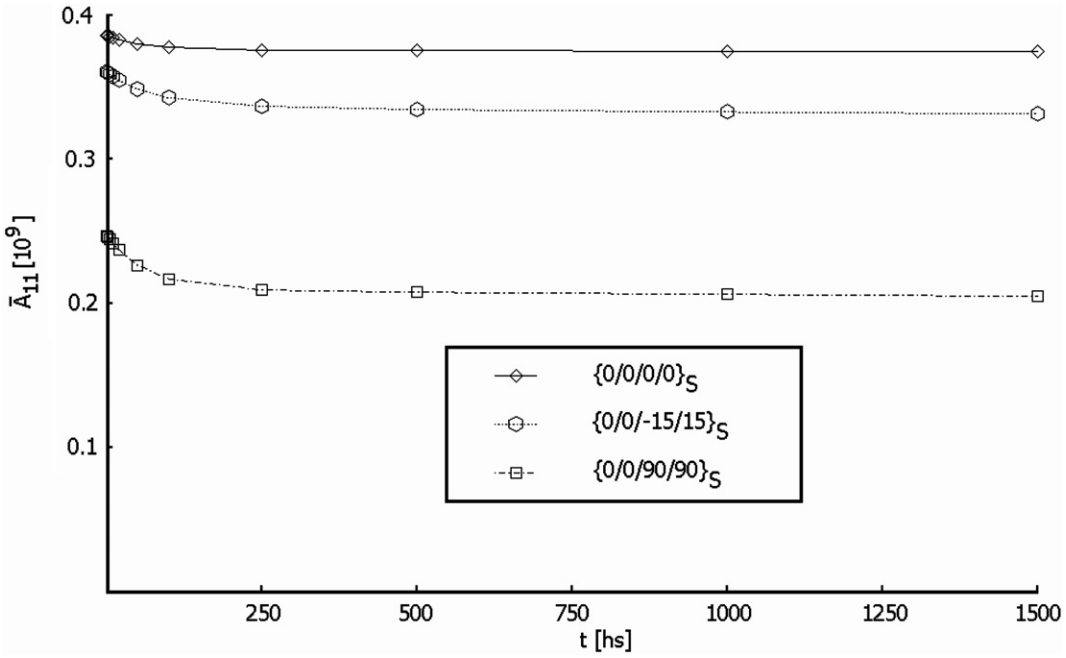

Fig. 21. Variation of the relaxation coefficient $\overline{A}_{11}$ for three different laminates employed in the curved beam with closed cross-section.

In Figs. 22 and 23 one can see, for different stacking sequences, the creep behavior of displacements $u_{zc}(L/2)$ and $\phi_x(L/2)$, respectively. Note that in the case where $\alpha = 30°$ the beam has the least creep displacements of all the analyzed configurations. In Fig. 24, the creep displacement $u_{zc}(L/2)$ with respect to the angle of fiber orientation.

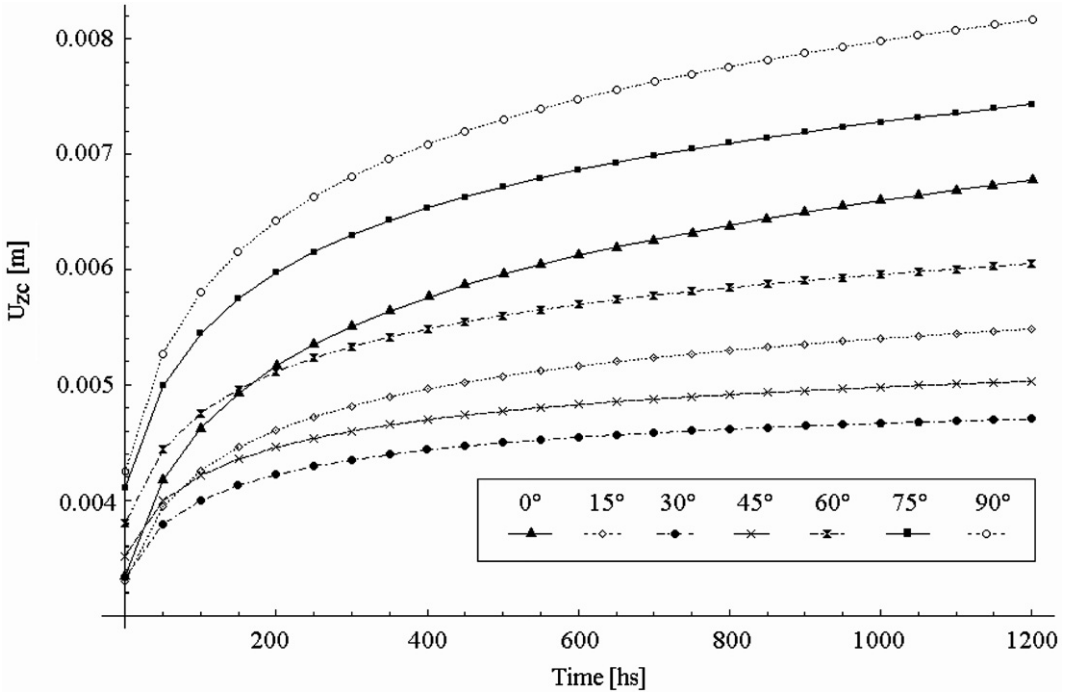

Fig. 22. Creep behavior of $u_{zc}(L/2)$ for the closed section.

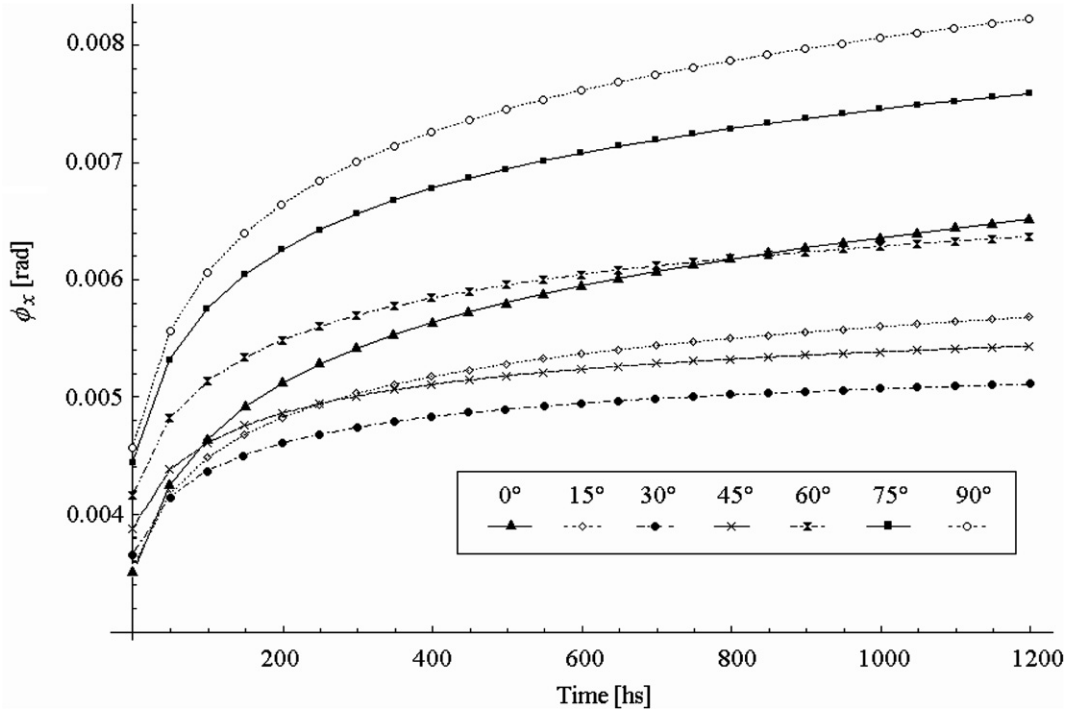

Fig. 23. Creep behavior of $\phi_x(L/2)$ for the closed section.

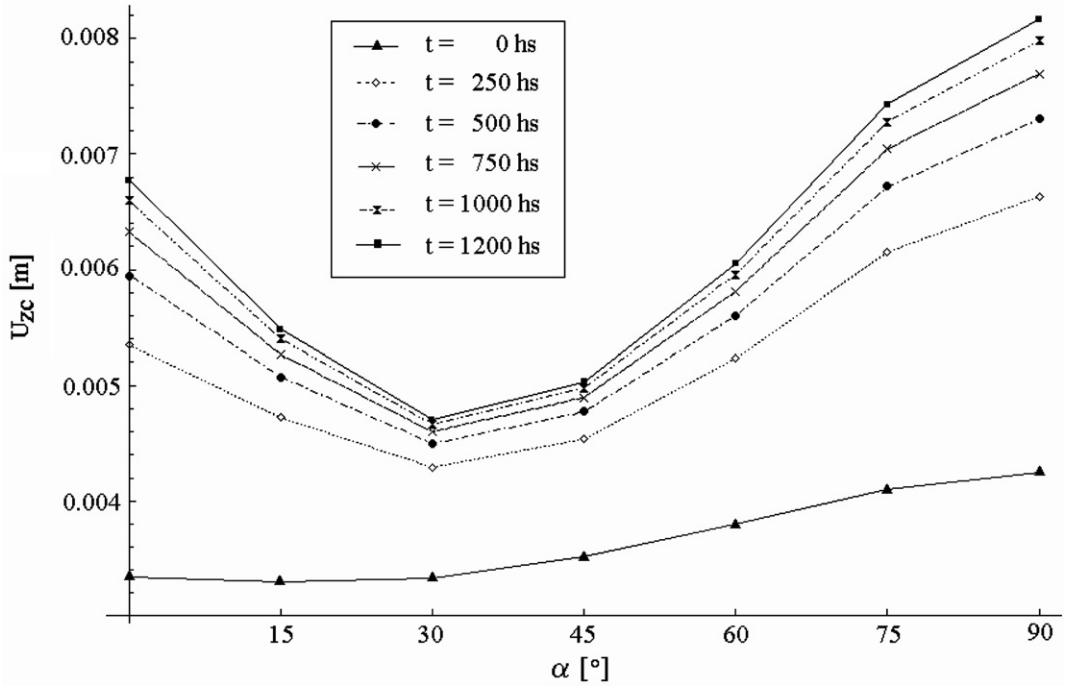

Fig. 24. Variation of $u_{zc}(L/2)$ with respect to the fiber orientation angle, for the closed section.

As one can see in the previous study, there is a fiber orientation angle which provides the least deflections in the beam for a given stacking sequence and for a given load condition. In the following study, the creep behavior of curved beams with different types of generic stacking sequences is analyzed. The same geometric, mate-

Table 4
Angle of fiber reinforcement, for different generic stacking sequences, that manifest better creep behavior in a case of curved beam with closed cross-section

Type of generic stacking sequence	Angle for best performance of	
	$u_{zc}(L/2)$	$\phi_x(L/2)$
Symmetric balanced $\{\alpha/-\alpha/-\alpha/\alpha\}_S$	15	15
CUS: $\{0/\alpha\}_4$	30	30
CAS: $\{\alpha/\alpha\}_4$ and $\{-\alpha/-\alpha\}_4$ top and bottom flanges $\{\alpha/-\alpha\}_4$ and $\{-\alpha/\alpha\}_4$ inner and outer webs	15	15

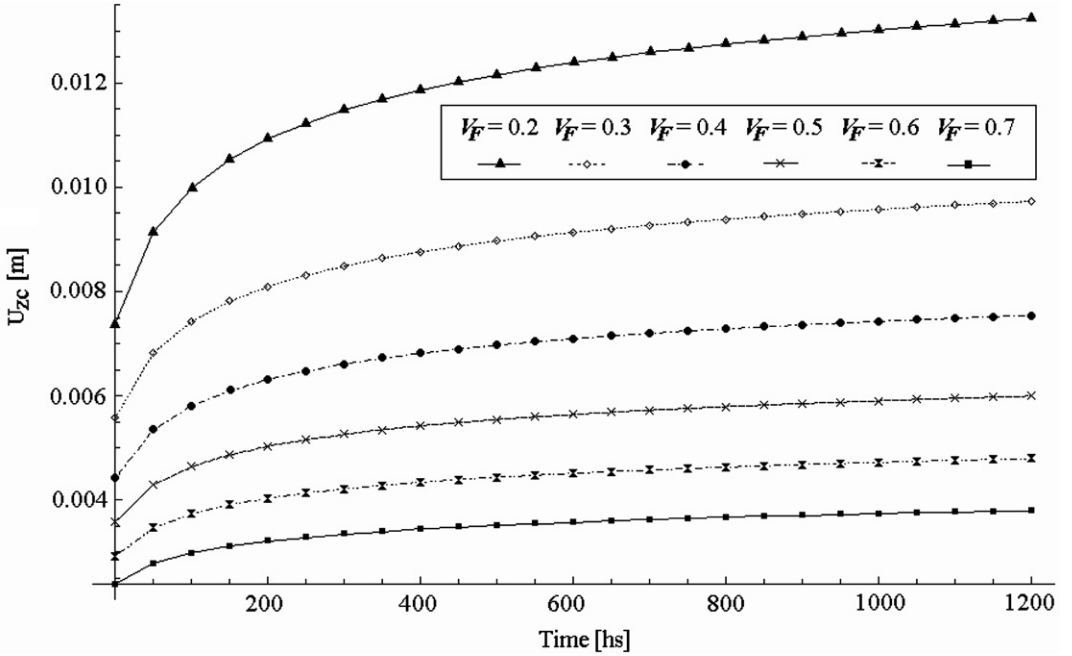

Fig. 25. Influence of the fiber volume fraction on the creep behavior of $u_{zc}(L/2)$, for the closed section.

rial, boundary conditions and loading features of the previous example are employed. However three types of generic stacking sequences are compared: symmetric balanced laminates, Circumferentially Uniform Stiffness laminates (denominated CUS) and Circumferentially Asymmetric Stiffness (denominated CAS). The angle α of fiber reinforcement can have the values 0°, 15°, 30°, 45°, 60°, 75°, or 90°, which are common in practical cases (Barbero, 1999; Jones, 1999). In Table 4 one can see the angle of fiber reinforcement that gives the best creep behavior for those generic stacking sequences and for the loading conditions imposed to the beam. It is interesting to note that for different generic stacking sequences angles of 15° and 30° offer the best performances of the seven values of angle α. Moreover if there is interest to obtain the angle for the best general creep performance, a scheme involving techniques of optimization has to be introduced.

The influence of the fiber volume fraction V_F on the creep behavior of the curved beam with a CUS stacking sequence when $\alpha = 15°$ is shown in Fig. 25. One can see that beam creep displacements have a stable variation over time for higher fiber volume fractions. On the other hand when the fiber volume fraction is increased from $V_F = 0.2$ to $V_F = 0.7$, the creep deflections can be reduced more than four times.

5. Conclusions

In the present paper, a model to predict the flexural–torsional creep behavior of thin-walled laminated FRP curved beams is presented. The motion equations for the curved beam member can be solved either analyti-

cally or numerically in the Carson domain. In order to solve general flexural–torsional coupled problems a finite element methodology was employed. The creep responses are obtained appealing to a numerical inversion of the Laplace transformation. A complete package was programmed in the environment of the software *Mathematica*, which offers the possibility to calculate in a unified fashion analytically or numerically the linear viscoelastic behavior of the curved beams. The model developed in this paper can be reduced to analyze the linear viscoelastic behavior of straight beams. In this particular option, it has shown a good correspondence with the predictions of other approaches for straight beams and with the available experimental data. Parametric studies for curved beams with open and closed cross-sections were performed. In these studies the importance of certain stacking sequences in what concerns to especial elastic couplings for both open and closed sections was appropriately enhanced. From these studies it was possible to show that for certain types of generic stacking sequences there are certain angles for fiber reinforcement that provides the best creep behavior, meaning that the beam has the least deflections. This is important in order to evaluate a beam design and to select a particular stacking sequence.

Acknowledgements

The present study was sponsored by Secretaría de Ciencia y Tecnología de la Universidad Tecnológica Nacional and CONICET.

References

Aboudi, J., 1991. Mechanics of Composite Material, a Unified Micromechanical Approach. Elsevier Inc., New York.

Barbero, E.J., 1999. Introduction to Composite Material Design. Taylor and Francis Inc.

Barbero, E.J., 2007. Finite Element Analysis of Composite Materials. CRC Press, Taylor and Francis Group.

Barbero, E.J., Lopez-Anido, R., Davalos, J.F., 1993. On the mechanics of thin-walled laminated composite beams. Journal of Composite Materials 27, 806–829.

Barbero, E.J., Luciano, R., 1995. Micromechanical formulas for the relaxation tensor of linear viscoelastic composites with transversely isotropic fibers. International Journal Solids and Structures 32 (13), 1859–1872.

Chandra, R., Stemple, A.D., Chopra, I., 1990. Thin walled composite beams under bending, torsional and extensional loads. Journal of Aircraft 27, 619–626.

Cortínez, V.H., Piovan, M.T., 2001. Analisis dependiente del tiempo de vigas de pared delgada construidas con materials compuestos. In: Mecánica Computacional, vol. 20, pp. 290–297.

Cortínez, V.H., Piovan, M.T., 2002. Vibration and buckling of composite thin walled beams with shear deformability. Journal of Sound and Vibration 258 (4), 701–723.

Harris, J.H., Barbero, E.J., 1998. Prediction of creep properties of laminated composites from matrix creep data. Journal of Reinforced Plastics and Composites 17 (4), 361–378.

Jones, R.M., 1999. Mechanics of Composite Materials. Taylor and Francis Inc.

Kim, C., White, S.R., 1997. Thick Walled composite beam theory including 3D elastic effects and torsional warping. International Journal Solids and Structures 34 (31–32), 4237–4259.

Laws, N., McLaughlin, J.R., 1978. Self-consistent estimates for the viscoelastic creep compliance of composite materials. Proceedings of the Royal Society, London 39, 251–273.

Lee, O., Ueng, C.E.S., 1995. Creep phenomenon of simple composite structures. Journal of Composite Materials 29 (15), 2069–2089.

Luciano, R., Barbero, E.J., 1994. Formulas for the stiffness of composites with periodic microstructure. International Journal Solids and Structures 31 (21), 2933–2944.

Luciano, R., Barbero, E.J., 1995. Analytical expressions for the relaxation moduli of linear viscoelastic composites with periodic microstructure. Journal of Applied Mechanics ASME 62 (3), 786–793.

Mallet, A., 2002. Numerical Inversion of Laplace Transform, Mathsource. Web Resources of Wolfram Research Inc.

Massa, J.C., Barbero, E.J., 1998. A strength of materials formulation for thin walled composite beams with torsion. Journal of Composite Materials 32 (17), 1560–1594.

Mase, G., 1977. Mecánica del Medio Contínuo. Compendios Schawm-McGraw-Hill. McGraw-Hill, Mexico.

Oliveira, B.F., Creus, G.J., 2003. Nonlinear viscoelastic analysis of thin walled beams in composite material. Thin-Walled Structures 41, 957–971.

Oñate, E., 1992. Cálculo de Estructuras por el método de elementos finitos, análisis estático lineal. CIMNE, Barcelona, Spain.

Piovan, M.T., Cortínez, V.H., 2002. Comportamiento viscoelástico lineal de vigas curvas anisótropas deformables por corte. In: Mecánica Computacional, vol. 21, pp. 1750–1769.

Piovan, M.T., Cortínez, V.H., 2003a. Mechanics of anisotropic curved beams with thin-walled sections (in Spanish). Revista Internacional de Métodos Numéricos para Cálculo y Diseño en Ingeniería 19 (3), 341–362.

Piovan, M.T., Cortínez, V.H., 2003b. Análisis de reticulados espaciales de vigas anisótropas de paredes delgadas con matriz viscoelástica lineal. In: Mecánica Computacional, vol. 22, pp. 564–579.

Piovan, M.T., Cortínez, V.H., 2005. Closed form solutions for composite thin-walled curved beams under static loadings. In: Proceedings of Cilamce XXVI, ABCM, Guaraparí, ES, Brazil.

Piovan, M.T., Cortínez, V.H., 2007a. Mechanics of shear deformable thin-walled beams made of composite materials. Thin-Walled Structures 45 (1), 37–62.

Piovan, M.T., Cortínez, V.H., 2007b. Mechanics of thin-walled curved beams made of composite materials, allowing for shear deformability. Thin-Walled Structures 45 (9), 759–789.

Piovan, M.T., 2003. Theoretical and Computational Study in the Mechanics of Composite Thin Walled Curved Beams, Considering Non-Conventional Effects. PhD Thesis. Department of Engineering, Universidad Nacional del Sur. Bahía Blanca, Argentina (in spanish).

Pollock, G., Sack, A., 1995. Shear center for elastic thin walled composite beams. Structural Engineering and Mechanics 3 (1), 91–103.

Qiao, P., Barbero, E.J., Davalos, J.F., 2000. On the linear viscoelasticity of thin walled laminated composite beams. Journal of Composite Materials 34, 39–68.

Smith, E.C., Chopra, I., 1991. Formulation and evaluation of an analytical model for composite box-beams. Journal American Helicopter Society 36 (3), 23–35.

Stemple, A.D., Lee, S.W., 1988. Finite-element model for composite beams with arbitrary cross-sectional warping. AIAA Journal 26 (12), 1512–1520.

Volovoi, V.V., Hodges, D.H., Berdichevsky, V.L., Sutyrin, V.G., 1999a. Asymptotic theory for static behavior of elastic anisotropic I beams. International Journal of Solids and Structures 36, 1017–1043.

Volovoi, V.V., Hodges, D.H., Cesnik, C.E.S., Popescu, B., 1999b. Assessment of beam modeling methods for rotor blade applications. In: Journal of the American Helicopter Society, 55th Annual Forum, Montreal, Que., Canada, May 25–27.

Wolfram, S., 1999. Mathematica, a system for doinf mathematics by computer. Addison-Wesley Publishing Company, New York.

Yu, W., Hodges, D.H., Volovoi, V.V., Fuchs, E.D., 2005. A generalized Vlasov theory for composite beams. Thin-Walled Structures 43, 1493–1511.

Zienkiewicz, O., 1980. Introducción al método de elementos finitos. Reverté, Barcelona, Spain.